

# BiF/NF<sub>2</sub> Kinetics Studies: Mechanism and Conversion Efficiency

Prepared by

R. F. HEIDNER III, J. S. HOLLOWAY, and J. B. KOFFEND  
Aerophysics Laboratory  
Laboratory Operations

31 August 1990

Prepared for

WEAPONS LABORATORY  
Kirtland Air Force Base, NM 87117

SPACE SYSTEMS DIVISION  
AIR FORCE SYSTEMS COMMAND  
Los Angeles Air Force Base  
P.O. Box 92960  
Los Angeles, CA 90009-2960

AD-A230 222

DTIC  
ELECTE  
DEC 20 1990

Co

Development Group

THE AEROSPACE CORPORATION  
El Segundo, California

APPROVED FOR PUBLIC RELEASE;  
DISTRIBUTION IS UNLIMITED

This report was submitted by The Aerospace Corporation, El Segundo, CA 90245-4691, under Contract No. F04701-88-C-0089 with the Space Systems Division, P. O. Box 92960, Los Angeles, CA 90009-2960. It was reviewed and approved for The Aerospace Corporation by R. W. Fillers, Director, Aerophysics Laboratory. Captain Rafael Riviere was the Air Force project officer for the Mission-Oriented Investigation and Experimentation (MOIE) program.

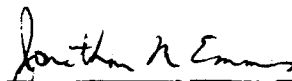
This report has been reviewed by the Public Affairs Office (PAS) and is releasable to the National Technical Information Service (NTIS). At NTIS, it will be available to the general public, including foreign nationals.

This technical report has been reviewed and is approved for publication. Publication of this report does not constitute Air Force approval of the report's findings or conclusions. It is published only for the exchange and stimulation of ideas.



---

RAFAEL RIVIERE, CAPT, USAF  
MOIE Project Officer  
SSD/CNL



---

JONATHAN M. EMMES, MAJ, USAF  
MOIE Program Manager  
AFSTC/WCO OL-AB

<b>REPORT DOCUMENTATION PAGE</b>				
1a. REPORT SECURITY CLASSIFICATION <b>Unclassified</b>		1b. RESTRICTIVE MARKINGS		
2a. SECURITY CLASSIFICATION AUTHORITY		3. DISTRIBUTION/AVAILABILITY OF REPORT <b>Approved for public release; distribution is unlimited.</b>		
2b. DECLASSIFICATION/DOWNGRADING SCHEDULE				
4. PERFORMING ORGANIZATION REPORT NUMBER(S) <b>TR-0090(5604)-1</b>		5. MONITORING ORGANIZATION REPORT NUMBER(S) <b>SSD-TR-90-34</b>		
6a. NAME OF PERFORMING ORGANIZATION <b>The Aerospace Corporation Laboratory Operations</b>		6b. OFFICE SYMBOL <i>(if applicable)</i>	7a. NAME OF MONITORING ORGANIZATION <b>Space Systems Division</b>	
6c. ADDRESS (City, State, and ZIP Code) <b>El Segundo, CA 90245-4691</b>		7b. ADDRESS (City, State, and ZIP Code) <b>Los Angeles Air Force Base Los Angeles, CA 90009-2960</b>		
8a. NAME OF FUNDING/SPONSORING ORGANIZATION <b>Weapons Laboratory</b>		8b. OFFICE SYMBOL <i>(if applicable)</i>	9. PROCUREMENT INSTRUMENT IDENTIFICATION NUMBER <b>F04701-88-C-0089</b>	
8c. ADDRESS (City, State, and ZIP Code) <b>Kirtland Air Force Base, NM 87117</b>		10. SOURCE OF FUNDING NUMBERS		
		PROGRAM ELEMENT NO.	PROJECT NO.	TASK NO.
		WORK UNIT ACCESSION NO.		
11. TITLE (Include Security Classification) <b>BiF/NF<sub>2</sub> Kinetics Studies: Mechanism and Conversion Efficiency</b>				
12. PERSONAL AUTHOR(S) <b>Heidner, Raymond F.; Holloway, John S.; and Koffend, John B.</b>				
13a. TYPE OF REPORT		13b. TIME COVERED FROM _____ TO _____		14. DATE OF REPORT (Year, Month, Day) <b>1990 August 31</b>
15. PAGE COUNT <b>36</b>				
16. SUPPLEMENTARY NOTATION				
17. COSATI CODES			18. SUBJECT TERMS (Continue on reverse if necessary and identify by block number) <b>Chemical Kinetics, Chemical Laser, Reaction Mechanics, Nitrogen Fluoride, Bismuth Fluoride.</b>	
FIELD	GROUP	SUB-GROUP		
19. ABSTRACT (Continue on reverse if necessary and identify by block number) <p>A series of experiments have been performed which examine the phenomenology of the formation of electronically excited BiF(AO<sup>+</sup>) in a photoinitiated reaction sequence involving NF<sub>2</sub>, H<sub>2</sub>, and Bi atoms at 450 K. The experiments are based on time resolved, absolutely calibrated detection of three key reactive intermediates; BiF(AO<sup>+</sup>), NF(a<sup>1</sup>Δ), and Bi(<sup>2</sup>D<sub>3/2</sub>). The results of these measurements are not found to be consistent with the currently accepted formation mechanism. An alternative mechanism in which a metastable state of BiF serves as an intermediate in the production of the A state is discussed in light of recent theoretical and experimental spectroscopic studies. Estimates are also made of the efficiency with which the electronic energy of NF(a<sup>1</sup>Δ) is converted to BiF (A→X) photons, and the degree to which Bi/BiF is repetitively pumped to the A state.</p>				
20. DISTRIBUTION/AVAILABILITY OF ABSTRACT <input checked="" type="checkbox"/> UNCLASSIFIED/UNLIMITED <input type="checkbox"/> SAME AS RPT. <input type="checkbox"/> DTIC USERS			21. ABSTRACT SECURITY CLASSIFICATION <b>Unclassified</b>	
22a. NAME OF RESPONSIBLE INDIVIDUAL		22b. TELEPHONE (Include Area Code)		22c. OFFICE SYMBOL

# CONTENTS

I. INTRODUCTION .....	5
II. EXPERIMENTAL .....	7
III. ABSOLUTE CALIBRATION .....	9
IV. RESULTS AND DISCUSSION .....	13
A. Detection of Bi Using Laser-Induced Fluorescence .....	13
B. Detection of Bi Using Absorption .....	15
C. Kinetics Results .....	18
V. CONCLUSIONS .....	29
REFERENCES .....	31
APPENDIX. KINETIC MODEL .....	33



Accession for	
NHS CRAM	<input checked="" type="checkbox"/>
Doc 148	<input type="checkbox"/>
Unprocessed	<input type="checkbox"/>
Justification	
By	
Date	
Availability Codes	
Dist	Avail. to/for Special
<b>A-1</b>	

## FIGURES

1.	Schematic Diagram of Experimental Apparatus .....	8
2.	Measured Filter Transmission Curves and Pertinent $NF(a^1\Delta)$ , $Bi(^2D_{3/2})$ , and $BiF(A0^+)$ Emission Features .....	10
3.	$Bi(^2D_{3/2})$ Time Profiles from 249-nm Photolysis of $Bi(CH_3)_3$ in Argon ( $[Ar] = 2.7 \times 10^{17}$ atoms/cm <sup>3</sup> ; $[Bi(CH_3)_3] = 1.6 \times 10^{13}$ molecules/cm <sup>3</sup> ) .....	14
4.	$Bi\ ^4P_{3/2} \rightarrow\ ^2D_{5/2}$ Laser Induced Fluorescence as a Function of Dye Laser Power .....	16
5.	$Bi(^2D_{3/2})$ Decay Rates as a Function of $Bi(CH_3)_3$ Density from KrF Laser Photolysis .....	17
6.	Experimental Determinations of the Absorption Cross Section $\sigma$ for the $7s\ ^4P_{3/2} \leftarrow 6p^3\ ^2D_{3/2}$ Bi Atom Transition at 298.99 nm .....	19
7.	Experimental $NF(a^1\Delta)$ , $BiF(A0^+)$ , and $Bi(^2D_{3/2})$ Time Profiles .....	20
8.	Excited State Time Histories of $NF(a^1\Delta)$ , $BiF(A0^+)$ , and $Bi(^2D_{3/2})$ .....	21
9.	Plot of Eq. (II) Constructed from the Absolute Data Presented in Fig. 8 .....	23
10.	Steady-State Plot Suggested by Eq. (II) Calculated Using the Kinetic Model Presented in the Appendix .....	23
11.	Zero-Point Energies of the Lowest Lying States of $BiF$ According to Ref. 2 and the More Recent Assignment of Ref. 20 .....	25

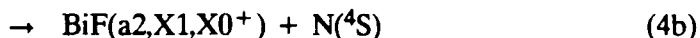
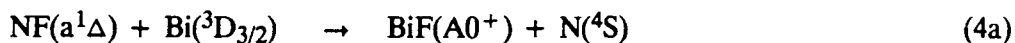
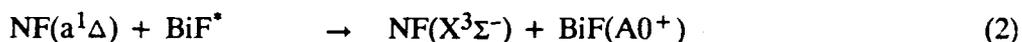
## TABLES

1.	Total Integrated $BiF(A)$ Photon Emission .....	27
----	---	----

## I. INTRODUCTION

Unraveling the complex kinetics of the  $\text{NF}(a^1\Delta)/\text{BiF}(A0^+)$  energy transfer system has been an ongoing concern of our laboratory for the past several years. The system is of particular interest because of its potential as a visible chemical laser. Of central importance in the evaluation of this potential is a knowledge of the chemical pathways leading to the formation of electronically excited  $\text{BiF}(A0^+)$ . This report describes the results of a series of recent experiments designed to investigate the nature of the  $\text{BiF}(A0^+)$  production mechanism and the efficiency with which the electronic energy of  $\text{NF}(a^1\Delta)$  is converted to  $\text{BiF}(A \rightarrow X)$  photons. We have examined the time behavior of three key species resulting from excimer laser initiated reactions of  $\text{NF}_2/\text{Bi}(\text{CH}_3)_3$ ,  $\text{NF}_2/\text{Bi}(\text{CH}_3)_3/\text{H}_2$ , and  $\text{NF}_2/\text{Bi}(\text{CH}_3)_3/\text{HBr}$  mixtures. An absolute calibration of the detection sensitivity for  $\text{NF}(a^1\Delta)$ ,  $\text{BiF}(A0^+)$ , and  $\text{Bi}(^2D_{3/2})$  was used to determine absolute number densities from time resolved emission, absorption, and laser induced fluorescence data.

Energy conservation dictates that at least two  $\text{NF}(a^1\Delta)$  molecules ( $T_e = 1.42 \text{ eV}$ ) are required to produce one  $\text{BiF}(A0^+)$  ( $T_e = 2.85 \text{ eV}$ ). At low Bi and  $\text{NF}(a)$  densities, where the removal of  $\text{BiF}(A0^+)$  is dominated by spontaneous emission (Ref. 1), the production of  $\text{BiF}(A0^+)$  scales as  $[\text{NF}(a^1\Delta)]^2$ . This observed scaling has led to the proposal of two simple models to account for  $\text{BiF}(A0^+)$  production:



Processes (1) - (4) are not all inclusive of the reaction and quenching channels; however they are sufficient to illustrate the requirements of the pumping mechanism.

The identity of the  $\text{BiF}^*$  state invoked in Mechanism 1 has been a matter of considerable speculation. Based on the spectroscopic work of Jones and McLean (Ref. 2) and of Chakoo and Patel (Ref. 3), the state had been tentatively identified (in the nomenclature of Ref. 2) as  $\text{BiF}(b0^+)$  ( $T_e = 1.14 \text{ eV}$ ). In order for the successive energy transfers of Processes (1) and (2) to take place within  $kT$  of resonance, the receptor level of the  $\text{BiF}(b0^+)$  state would necessarily have to be  $v' = 4$ . Previous experiments (Ref. 4) showed that the yield of  $\text{BiF}(A0^+)$  was independent of Ar buffer gas pressure. This result was taken as an indication that a vibrationally excited intermediate (which could be collisionally relaxed) was not involved.

Accordingly, our attention has been focused on Mechanism 2, which does not involve a vibrationally excited state. Support for this mechanism also comes from the fact that Reaction (3) is well known (Ref. 5) and extremely efficient ( $k_3 = 2 \times 10^{-10}$  cm<sup>3</sup>/molecule-sec).<sup>1</sup> The Bi(<sup>2</sup>D<sub>3/2</sub>) intermediate is optically metastable and collisionally inert with most partners. The purpose of the current experiments was to measure the time behavior of three important species for comparison with predictions based on Mechanism 2. However, as will be shown, under our experimental conditions, BiF(A0<sup>+</sup>) formation by Mechanism 2 is not consistent with our data. Based on the results of these experiments and new spectroscopic information on BiF, reconsideration of other BiF(A0<sup>+</sup>) production mechanisms is required.

## II. EXPERIMENTAL

A diagram of the experimental apparatus is given in Fig. 1. Experiments were carried out in a heated stainless steel cell maintained at 170°C. Flow rates were determined using calibrated mass flowmeters (Tylan). A 10% mixture of N<sub>2</sub>F<sub>4</sub> in Ar was flowed through a quartz bulb kept at 190°C to ensure complete pyrolysis into NF<sub>2</sub>. Other reagents were flowed directly into the photolysis cell. A 249-nm KrF laser pulse was used to initiate reactions from NF<sub>2</sub>/Bi(CH<sub>3</sub>)<sub>3</sub>/Ar and NF<sub>2</sub>/H<sub>2</sub>/Bi(CH<sub>3</sub>)<sub>3</sub>/CO<sub>2</sub>/Ar mixtures, while a 193-nm ArF laser was used for mixtures containing NF<sub>2</sub>/HBr/Bi(CH<sub>3</sub>)<sub>3</sub>/CO<sub>2</sub>/Ar. The excimer laser was operated at repetition rates of 1–2 Hz to permit replacement of the gas mixture in the photolysis cell between laser shots. Both NF(a<sup>1</sup>Δ) and BiF(A0<sup>+</sup>) were detected by time resolved emission using a thermoelectrically cooled GaAs photomultiplier tube (PMT) (RCA C31034) and an "S" response PMT (EMI 6256S), respectively. Narrow bandpass filters were employed to isolate the emission from the NF a-X (0,0) band at 874 nm and the BiF A-X (0,2) band at 457 nm. Three methods were used for Bi(<sup>2</sup>D<sub>3/2</sub>) detection:

- In some cases, Bi(<sup>2</sup>D<sub>3/2</sub>) was monitored directly in emission by the <sup>2</sup>D<sub>3/2</sub> - <sup>4</sup>S<sub>3/2</sub> transition at 876 nm using an additional cooled GaAs PMT and narrow-band filter.
- A single-mode ring dye laser (Coherent model CR-699-21) using Rhodamine 6G dye was intracavity frequency doubled to provide 0.5 - 3 mW of radiation near 300 nm with a bandwidth of 1 MHz. The dye laser was used to monitor Bi(<sup>2</sup>D<sub>3/2</sub>) using laser induced fluorescence (LIF) by pumping the Bi <sup>4</sup>P<sub>3/2</sub> ← <sup>2</sup>D<sub>3/2</sub> transition at 298.9 nm. The resulting Bi <sup>4</sup>P<sub>3/2</sub> → <sup>2</sup>D<sub>5/2</sub> fluorescence at 339.7 nm was detected using a second "S" response PMT (EMI 6256S) equipped with an 8-nm FWHM bandpass filter centered at 340 nm.
- In addition, Bi(<sup>2</sup>D<sub>3/2</sub>) was also observed by its absorption on the 7s <sup>4</sup>P<sub>3/2</sub> - 6p<sup>3</sup> <sup>2</sup>D<sub>3/2</sub> transition. Light from a Bi hollow cathode lamp, collimated with a 10-cm focal lens, was directed longitudinally through the photolysis cell and focused on the slits of a 1/3 meter monochromator (McPherson 218). The Bi line emission was detected by a PMT (Hamamatsu R2658) mounted on the exit slit of the monochromator. The monochromator was operated with a spectral bandpass of 0.2 nm, adequate to resolve the Bi <sup>4</sup>P<sub>3/2</sub> ← <sup>2</sup>D<sub>3/2</sub> line from neighboring transitions. The Bi hollow cathode lamp was operated in a pulsed mode to provide sufficient intensity for time-resolved absorption measurements. Typically, the lamp pulse width was 500 μsec with a lamp current of 0.5 A during the pulse.

Emission, LIF, and absorption signals were acquired using a multichannel transient digitizer (LeCroy 2264) and stored with a laboratory computer (DEC LSI 11/73).

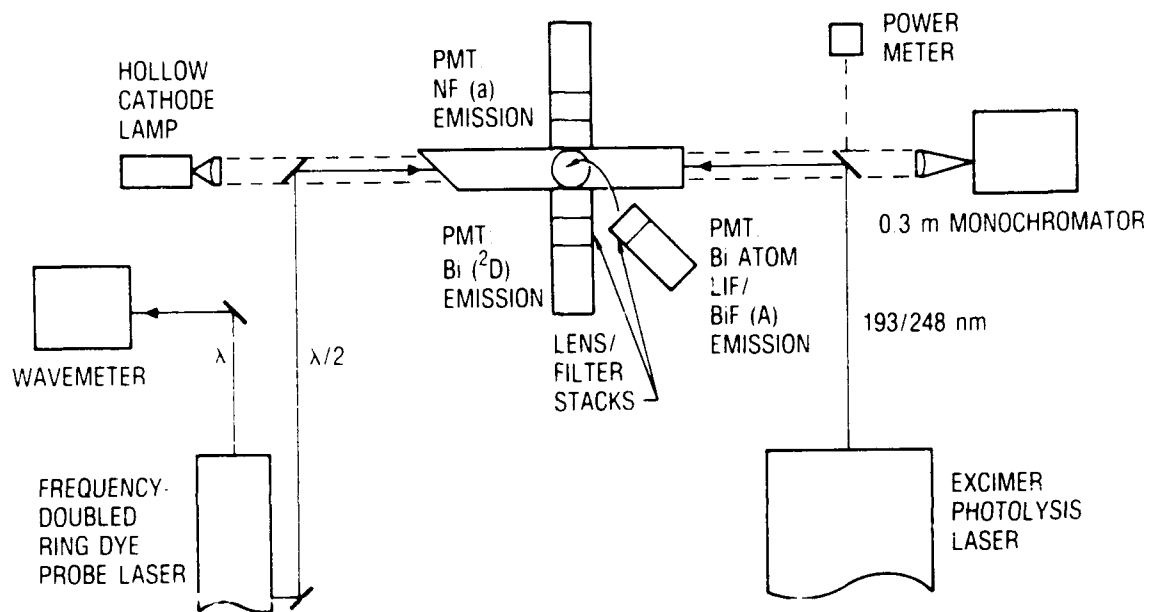


Fig. 1. Schematic Diagram of Experimental Apparatus.

### III. ABSOLUTE CALIBRATION

In order to obtain a relative calibration of PMT detection sensitivity for the species of interest, it is necessary to determine several detection characteristics. These include filter transmission curves and the relative wavelength responsivity of the various photomultiplier tubes. Three different detectors were used. The response of each PMT viewing the same signal provided the basis for a relative calibration among the three. Overlap of the emission spectrum of each species with its associated filter transmission curve and oscillator strengths of the various transitions must be employed in order to relate the light intensity incident on each detector to the number density of a particular species. Absolute calibration was accomplished by employing NF(a<sup>1</sup>Δ) emission from a known concentration of NF(a<sup>1</sup>Δ).

Transmission curves of the bandpass filters were measured with a quartz halogen lamp and a 1/3 meter monochromator using Ne lines from a spectral lamp to provide wavelength calibration. Since each filter had a very narrow bandpass,  $\Delta\lambda < 1$  nm, spectral variations in the intensity of the lamp could be neglected. Convolution of the filter transmission curves and the emission spectra of each species enabled us to determine the fraction of light from each emission feature transmitted through the different filters: the "filter response" factor. Figure 2 shows filter transmission curves near 874 nm along with the NF(a<sup>1</sup>Δ) and Bi(<sup>2</sup>D<sub>3/2</sub>) emission features. Also included in Fig. 2 is the BiF A-X filter transmission curve together with the pertinent part of the BiF A-X emission spectrum.

The relative wavelength response of one of the GaAs detectors was determined with a tungsten ribbon lamp, whose temperature was measured using an optical pyrometer. The ribbon lamp photon flux was calculated using a standard Planck blackbody function corrected by the emissivity of tungsten reported by Rutgers and DeVos (Ref. 6). Measurements were performed using each of the three filters to cover the three narrow wavelength regions that they defined. The relative intensity falling on the PMT photocathode was determined from a convolution of the modified blackbody function with the measured filter transmission curves. The fact that the measured response at the similar NF(a<sup>1</sup>Δ) and Bi(<sup>2</sup>D<sub>3/2</sub>) wavelengths (874.3 and 875.5 nm) was identical within experimental error and that the relative response at 874 and 457 nm agreed with previous measurements in this laboratory (Ref. 7) lends credence to our results. The relative detection sensitivity for each species was then obtained from the measured wavelength responsivity of the PMT, the "filter response" factor, and the Bi(<sup>2</sup>D<sub>3/2</sub>), BiF(AO<sup>+</sup>, v=0), and NF(a<sup>1</sup>Δ) radiative lifetimes (Refs. 8-10).

One GaAs PMT was calibrated as described above. Relative detection sensitivity of the other detectors was determined from the comparison of NF(a<sup>1</sup>Δ), Bi(<sup>2</sup>D<sub>3/2</sub>), and BiF A-X (0,2) emission signals resulting from KrF photolysis of identical NF<sub>2</sub>/Bi(CH<sub>3</sub>)<sub>3</sub>/Ar and Bi(CH<sub>3</sub>)<sub>3</sub>/Ar mixtures as the various filters were rotated among the different phototubes. Since these calibrations were performed in situ, variations in sensitivity due to detection geometry and collection efficiency are inherently included.

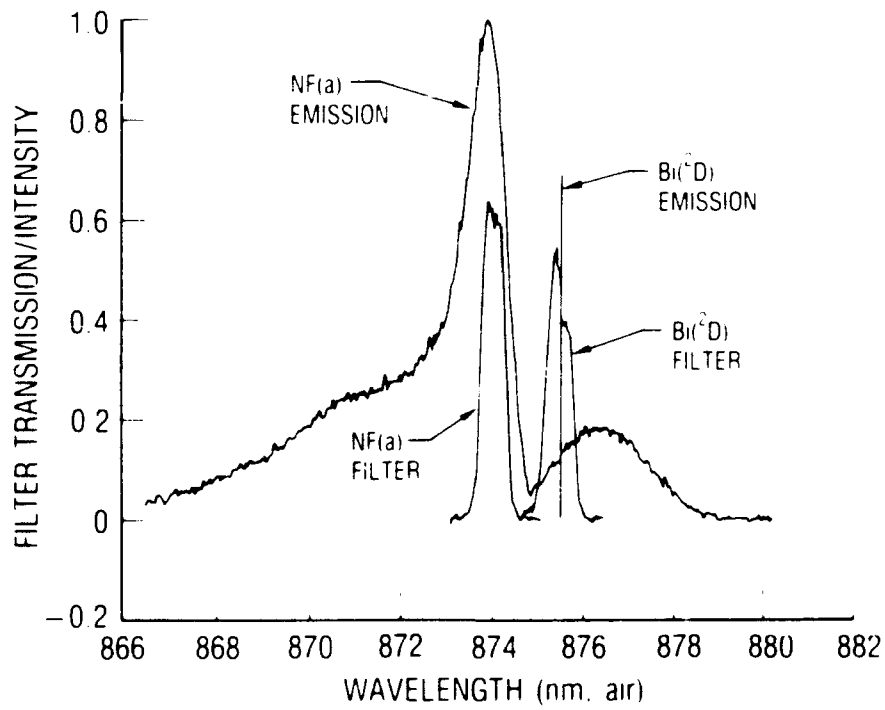
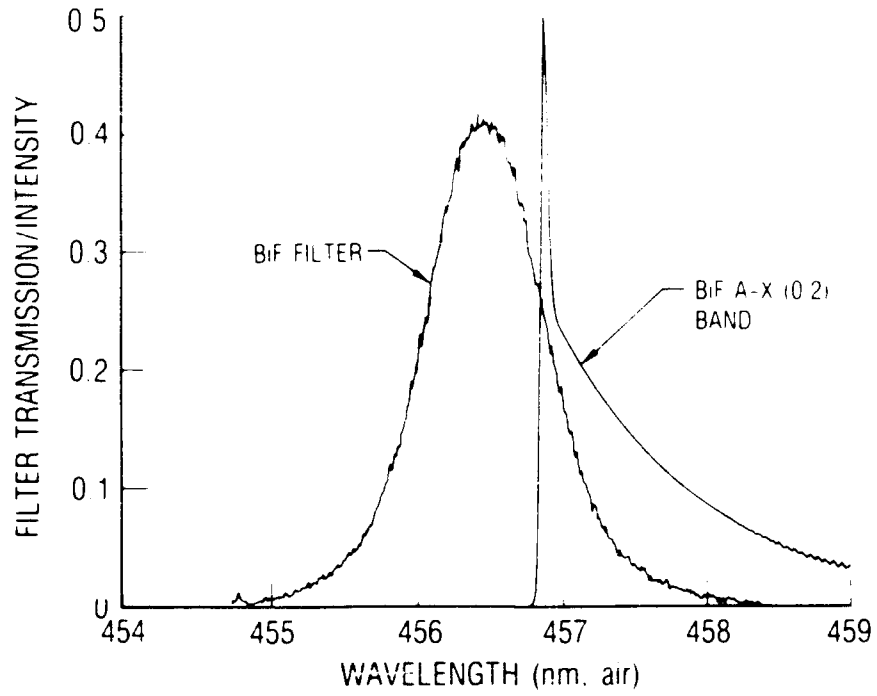


Fig. 2. Measured Filter Transmission Curves and Pertinent  $NF(a^1\Delta)$ ,  $Bi(^2D_{3/2})$ , and  $BiF(AO^+)$  Emission Features.

Absolute calibration of the detection sensitivity for  $\text{NF}(a^1\Delta)$  was performed using  $\text{NF}(a^1\Delta)$  emission signals from both the 249-nm photolysis of  $\text{NF}_2$  and the reaction of H atoms, created by HBr photolysis at 193 nm, with  $\text{NF}_2$ . The excimer laser beam profiles were determined from burn patterns, and the relative laser energy was measured using a Coherent model 212 power meter. Reported values for the  $\text{NF}_2$  (Refs. 11, 12) and HBr (Ref. 13) absorption cross sections at 249 and 193 nm, respectively, were used to calculate the  $\text{NF}_2$  and HBr photolysis fractions. We also performed our own measurement of the HBr absorption coefficient and reproduced the value given by Magnotta et al. (Ref. 13). The  $\text{NF}(a^1\Delta)$  photolysis quantum yield (Refs. 11, 12) and the  $\text{NF}(a^1\Delta)$  reaction branching ratio had both been previously determined (Refs. 10, 14). Thus, the  $\text{NF}(a^1\Delta)$  density could be calculated, and an absolute calibration was effected. The measurements of the  $\text{NF}(a^1\Delta)$  detection sensitivity from KrF laser photolysis of  $\text{NF}_2$  and from the 193-nm photolysis of HBr in  $\text{NF}_2$  differed by less than a factor of 2. Absolute detection sensitivities for  $\text{Bi}(^2D_{3/2})$  and  $\text{BiF}(A0^+, v' = 0)$  were then determined using the  $\text{NF}(a^1\Delta)$  result and the relative detection sensitivities described above.

The major contribution to the uncertainty in the absolute calibration stems from errors in the determination of the temperature of the tungsten ribbon lamp. The rather low operating temperature of 1700 K results in large errors in the calculated lamp flux at the  $\text{BiF A-X}(0,2)$  band wavelength for relatively small errors in the measured tungsten ribbon temperature. This primarily affects the determination of the relative wavelength response of the PMT at 860 and 457 nm. In addition, errors in the weak  $\text{Bi}(^2D_{3/2})$  ( $\tau = 31$  msec) (Ref. 8) and  $\text{NF}(a^1\Delta)$  ( $\tau = 5.5$  sec) (Ref. 10) transition strengths are also important. Taking these and other factors into consideration, we estimate that errors in our absolutely calibrated data are on the order of a factor of 2 for  $\text{Bi}(^2D_{3/2})$  and  $\text{NF}(a^1\Delta)$  data which occur at nearly adjacent wavelengths. An uncertainty of about a factor of 4 is estimated for the  $\text{BiF}(A0^+)$  as a result of the error involved in the temperature determination of the tungsten ribbon. While these uncertainties are significant, they do not obviate the major points made in Section IV.

## IV. RESULTS AND DISCUSSION

As discussed previously, this series of experiments was originally conceived as a means of testing (albeit under a limited range of conditions) the validity of the proposed mechanism for  $\text{BiF}(\text{A}0^+)$  production. Our means of accomplishing this objective was to ascertain the time histories of the excited state intermediates  $\text{Bi}(^2\text{D}_{3/2})$ ,  $\text{NF}(\text{a}^1\Delta)$ , and  $\text{BiF}(\text{A}0^+)$ . This was to be done by recording time-resolved traces of their optical emission. This is a valid approach for those experiments in which the KrF photolysis of  $\text{NF}_2$  is the predominant source of  $\text{NF}(\text{a}^1\Delta)$ . However, when the photolysis was employed to initiate the  $\text{H} + \text{NF}_2$  chemistry, the emission from the resulting  $\text{NF}(\text{a}^1\Delta \nu' = 1)$  is sufficient to obscure  $\text{Bi}(^2\text{D}_{3/2})$  emission. It was therefore necessary to develop alternative methods of monitoring  $\text{Bi}(^2\text{D}_{3/2})$ .

### A. DETECTION OF Bi USING LASER-INDUCED FLUORESCENCE

Attempts to monitor  $\text{Bi}(^2\text{D}_{3/2})$  by pumping the  $^4\text{P}_{1/2} - ^2\text{D}_{3/2}$  transition at 472.2 nm and observing  $^4\text{P}_{1/2} - ^4\text{S}$  LIF at 306.8 nm proved to be complicated by optical pumping and radiation trapping effects. At higher single-mode dye laser powers ( $\approx 300$  mW), an appreciable fraction of the  $\text{Bi}(^2\text{D}_{3/2})$  population was transferred to the  $^4\text{P}_{1/2}$  state. The use of lower dye laser powers diminished the optical pumping effects. However, as a consequence of the very high oscillator strength of the 306.8-nm Bi transition ( $gf = 0.99$ ) (Ref. 15) and high Bi  $^4\text{S}$  ground state density, radiation trapping precluded the use of this Bi detection method. An alternative LIF detection scheme was therefore chosen. In this case, the time history of  $\text{Bi}(^2\text{D}_{3/2})$  was observed by exciting the  $^4\text{P}_{3/2} - ^2\text{D}_{3/2}$  transition at 298.9 nm, with subsequent detection of  $^4\text{P}_{3/2} - ^2\text{D}_{5/2}$  emission at 339.7 nm. Since only very modest laser fluences were employed ( $\sim 1$  mW), optical pumping of the  $^2\text{D}_{3/2}$  state was avoided. Because only transitions between Bi excited states were involved, we observed no indication of radiation trapping.

Initial studies focused on the KrF laser photolysis of  $\text{Bi}(\text{CH}_3)_3/\text{Ar}$  mixtures where  $\text{Bi}(^2\text{D}_{3/2})$  was simultaneously monitored by time resolved emission at 876 nm, in addition to time-resolved LIF. Figure 3 contains experimental  $\text{Bi}(^2\text{D}_{3/2})$  traces resulting from both techniques. Clearly, the normalized  $\text{Bi}(^2\text{D}_{3/2})$  time profiles in Fig. 3 do not decay at the same rate; the LIF profile decays some 20–30% faster than the 876-nm emission profile. A systematic study of the  $\text{Bi}(^2\text{D}_{3/2})$  LIF was undertaken to obtain an explanation for this discrepancy.

The  $\text{Bi}(^2\text{D}_{3/2})$  LIF was recorded as the Ar buffer gas density was varied by nearly an order of magnitude from  $1 \times 10^{17}$  to  $8 \times 10^{17}$  atoms/cm<sup>3</sup> while holding the initial Bi atom density constant. The  $\text{Bi}(^2\text{D}_{3/2})$  LIF decay and amplitude remained constant. Similarly, the LIF decay and amplitude were invariant as the dye laser beam area was changed from 0.2 to 1.0 cm<sup>2</sup>. We may, therefore, conclude that the effects of Bi atom diffusion are negligible for our experimental conditions.

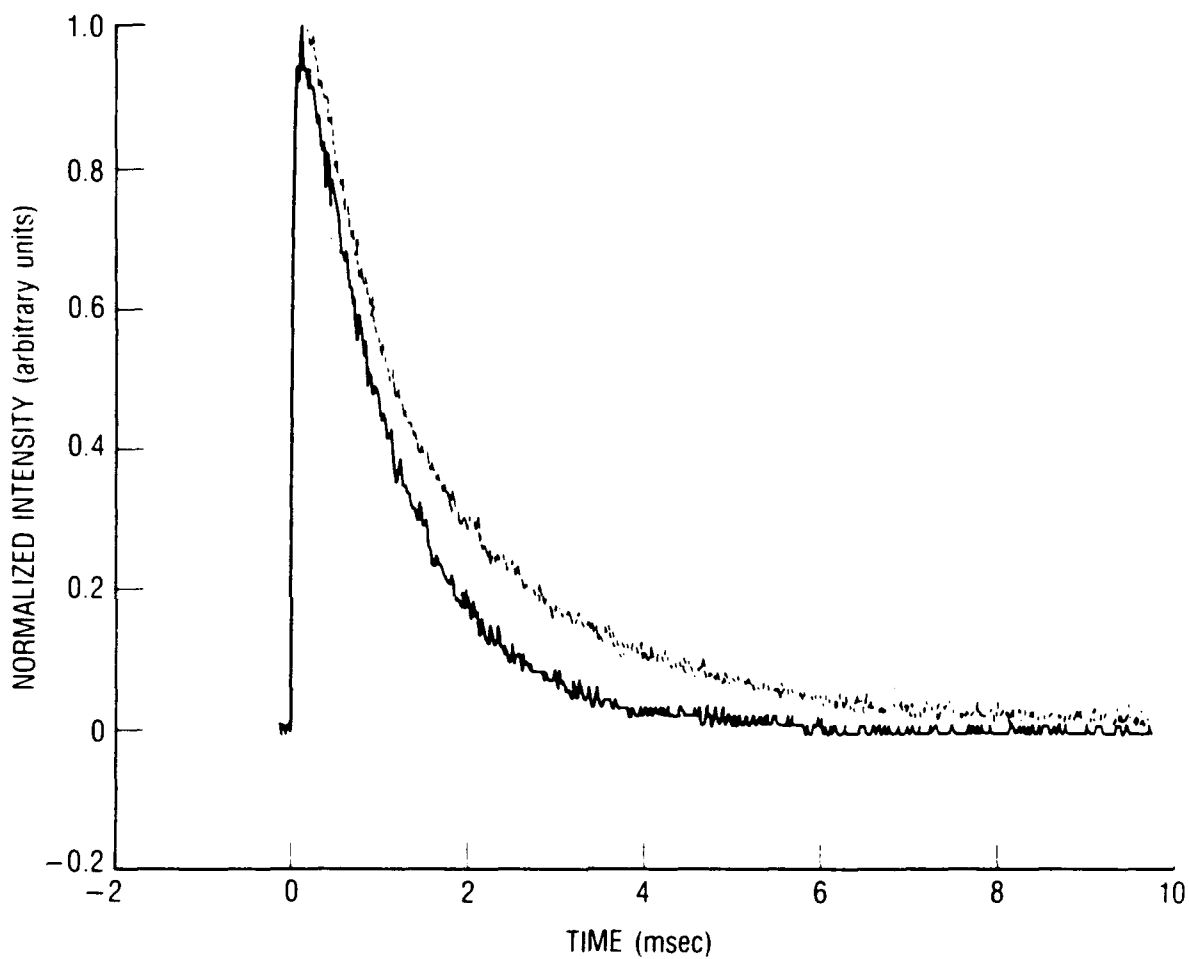


Fig. 3.  $\text{Bi}(^2\text{D}_{3/2})$  Time Profiles from 249-nm Photolysis of  $\text{Bi}(\text{CH}_3)_3$  in Argon ( $[\text{Ar}] = 2.7 \times 10^{17}$  atoms/cm<sup>3</sup>;  $[\text{Bi}(\text{CH}_3)_3] = 1.6 \times 10^{13}$  molecules/cm<sup>3</sup>). The dotted curve is  $\text{Bi}(^2\text{D}_{3/2}) - \text{Bi}(^4\text{S})$  emission, and the solid trace is the  $\text{Bi}^4\text{P}_{3/2} \rightarrow ^2\text{D}_{5/2}$  laser induced fluorescence.

The  $\text{Bi}(^2\text{D}_{3/2})$  LIF behaves as expected as a function of the dye laser power. Plots of the LIF amplitudes and decay rates are shown in Fig. 4 for several dye laser powers. The maximum dye laser power delivered to the photolysis cell was about 0.7 mW. The amplitude scales linearly with the dye laser power and passes through the origin, and the LIF decay rate remains constant for the entire range studied. Thus, optical pumping effects are absent for the dye laser fluences used in this study. This is supported by the observation that the  $\text{Bi}(^2\text{D}_{3/2})$  emission decay rate is unaffected by the presence of the dye laser, contrary to the results of 472-nm LIF experiments.<sup>‡</sup>

The rate coefficient for the quenching of  $\text{Bi}(^2\text{D}_{3/2})$  by  $\text{Bi}(\text{CH}_3)_3$  was measured using  $\text{Bi}(^2\text{D}_{3/2})$  time profiles obtained from both  $\text{Bi}(^2\text{D}_{3/2})$  emission and LIF. Experimental  $\text{Bi}(^2\text{D}_{3/2})$  profiles were fit to a single exponential function, and decay rates are plotted against  $\text{Bi}(\text{CH}_3)_3$  density in Fig. 5. The slopes of both curves agree within our experimental uncertainty. We also note that the rate constants obtained here are in reasonable agreement with those reported in Ref. 16. The difference between the emission and LIF data in Fig. 5 lies in the values of the intercept. The emission data pass within experimental error through the reported (Ref. 8)  $\text{Bi}(^2\text{D}_{3/2})$  Einstein A coefficient of  $31.2 \text{ sec}^{-1}$ . However, the intercept of the LIF data is nearly six times larger. The reason for this effect remains unexplained.

## B. DETECTION OF BI USING ABSORPTION

Because of anomalous results obtained from our LIF experiments, we chose to verify the results of our  $\text{Bi}(^2\text{D}_{3/2})$  measurements by means of an absorption probe on the  $^4\text{P}_{3/2} \leftarrow ^2\text{D}_{3/2}$  Bi atom transition at 298.9 nm. This is the same transition which was employed as the pumping step of our LIF probe. Because the species of interest is atomic, its absorption cross section is quite large. As a result, this method proved to be sufficiently sensitive at the rather low number densities used in these experiments. Absorption measurements are inherently quantitative. Analysis of the resultant data is straightforward, and absolute values for  $\text{Bi}(^2\text{D}_{3/2})$  densities may be determined by way of our previous calibrations.

For these experiments we have employed a pulsed Bi hollow cathode lamp (HCL). The use of an HCL provides a stable and reproducible atomic line source whose features are sharp and relatively unperturbed by electric field effects and pressure broadening (Ref. 17). The lamp was operated in the pulsed mode in order to provide sufficient intensity on the time scale of the excited state lifetimes.

To obtain absolute number densities, it was first necessary to determine an absorption cross section for the  $^4\text{P}_{3/2} \leftarrow ^2\text{D}_{3/2}$  Bi transition. This was accomplished by conducting a series of experiments in which varying densities of  $\text{Bi}(\text{CH}_3)_3$  were photolyzed at KrF wavelength. The resultant  $\text{Bi}(^2\text{D}_{3/2})$  population was monitored in both emission and absorption. Source intensity in the absence of absorption ( $I_0$ ) was determined both with the gas mixture in the cell and the photolysis laser blocked and in the presence of the laser with the cell evacuated. Both methods gave identical values for  $I_0$ , indicating that there was no appreciable attenuation due to the gas mixture. The background was taken before and after each concentration measurement to account for any drift

<sup>‡</sup> The observed  $\text{Bi}(^2\text{D}_{3/2}) - ^4\text{S}$  emission decay rate increased with the 472-nm dye laser present due to optical pumping into the  $\text{Bi}(^4\text{P}_{1/2})$  which has a radiative lifetime of 7 nsec.

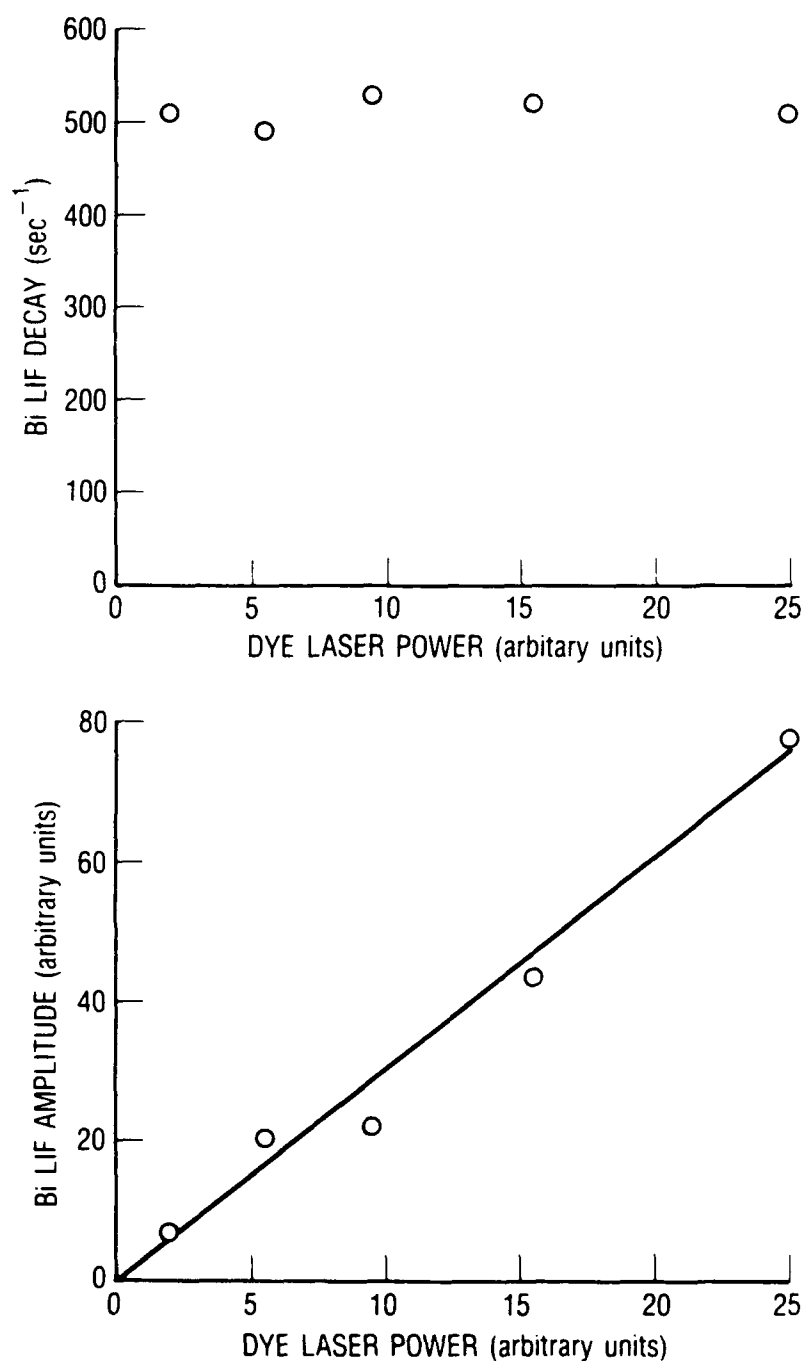


Fig. 4. Bi  $^4P_{3/2} \rightarrow ^2D_{5/2}$  Laser Induced Fluorescence as a Function of Dye Laser Power. Data are from the KrF laser photolysis of  $7.5 \times 10^{12}$  molecules/cm<sup>3</sup> Bi(CH<sub>3</sub>)<sub>3</sub> in  $2.6 \times 10^{17}$  atoms/cm<sup>3</sup> Ar. The upper part of the figure displays the decay rate behavior. The amplitude is shown in the lower part along with a linear fit constrained to pass through the origin. Decay rates and amplitudes are obtained from least-squares fits of time-resolved LIF data to a single exponential function.

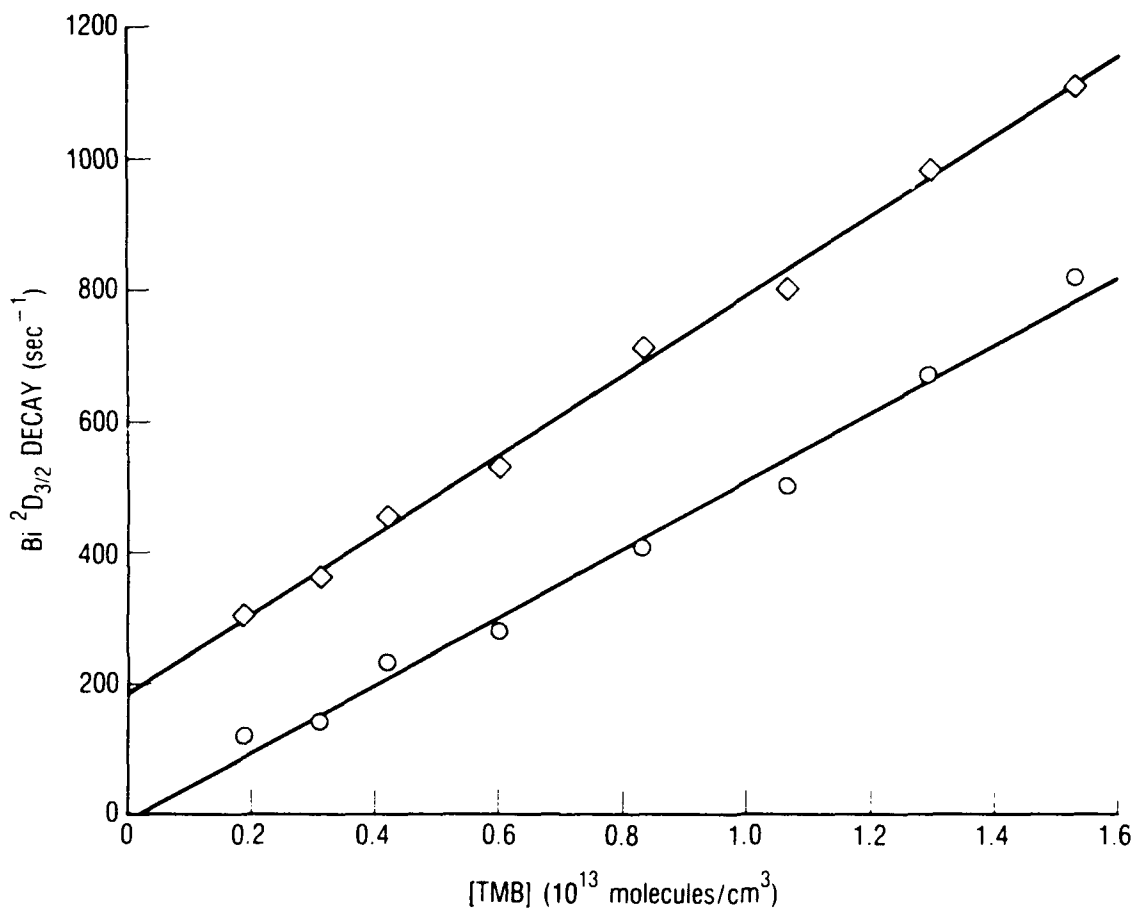


Fig. 5.  $\text{Bi}(^2D_{3/2})$  Decay Rates as a Function of  $\text{Bi}(\text{CH}_3)_3$  Density from KrF Laser Photolysis. The Ar concentration was held constant at  $1.8 \times 10^{17}$  atoms/cm $^3$ . Single exponential least-squares fits to the data provided the decay rates plotted. Diamonds represent the  $\text{Bi } ^4P_{3/2} \rightarrow ^2D_{5/2}$  LIF data, and  $\text{Bi}(^2D_{3/2})$  emission data are given by the circles. Slopes of the solid lines, linear fits to the data, are  $6.1 \pm 1.0 \times 10^{-11}$  cm $^3$ /molecule-sec (diamonds) and  $5.2 \pm 0.9 \times 10^{-11}$  cm $^3$ /molecule-sec (circles).

in the HCL signal or degradation in the transmission of the cell windows caused by slow accumulation of Bi metal from the photolysis. According to the Beer-Lambert expression

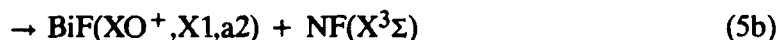
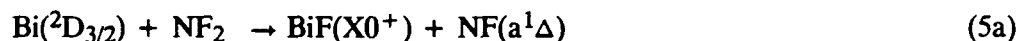
$$\sigma = \ln(I_0/I) / \{[\text{Bi}(^2\text{D}_{3/2})] l\} \quad (I)$$

where  $\sigma$  is the absorption cross section,  $I$  is the transmitted intensity, and  $l$  is the path length. Since we have absolutely calibrated the detection for  $\text{Bi}(^2\text{D}_{3/2})$  emission as discussed above, the absorption cross section can be determined from the emission and absorption data. Figure 6 shows the results for a number of experimental runs. We measure a value of  $\sigma = 3.7 \pm 1.4 \times 10^{-14} \text{ cm}^2$ . This value is over two orders of magnitude smaller than the cross section calculated based on the Einstein A coefficient for the transition (Ref. 15). This may be an indication that the lamp is self-reversed on this transition. However, as long as the operating conditions of the lamp are maintained constant, the use of our experimentally obtained cross section is valid in evaluating the absorption data.

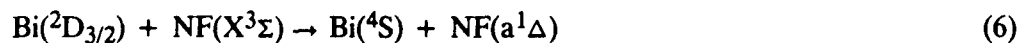
At higher  $\text{Bi}(\text{CH}_3)_3$  concentrations ( $> 6 \times 10^{13} \text{ molecules/cm}^3$ ), we observe a discrepancy in the temporal behavior of the absorption data with respect to the emission data. As with the anomalous results of the LIF experiments, the reason for this is not clear. Therefore, care was taken to conduct our subsequent experiments using  $\text{Bi}(\text{CH}_3)_3$  densities below  $5 \times 10^{13} \text{ molecules/cm}^3$  where both absorption and emission data yielded identical results.

### C. KINETICS RESULTS

Experimental time profiles of  $\text{Bi}(^2\text{D}_{3/2})$ ,  $\text{NF}(a^1\Delta)$ , and  $\text{BiF}(A0^+)$  from the KrF laser initiation of  $\text{NF}_2/\text{H}_2/\text{Bi}(\text{CH}_3)_3/\text{CO}_2/\text{Ar}$  mixtures using  $\text{Bi}(^2\text{D}_{3/2})$  LIF and absorption are presented in Figs. 7 and 8, respectively. Note that the  $\text{Bi}(^2\text{D}_{3/2})$  profiles obtained by both techniques decay on the same timescale. Because it occurs well within the induction time for the formation of  $\text{NF}(a^1\Delta)$ , the rapid  $\text{Bi}(^2\text{D}_{3/2})$  decay can be primarily attributed to reaction with  $\text{NF}_2$ .



A second removal channel for  $\text{Bi}(^2\text{D}_{3/2})$  is the reverse of Process (3), i.e.,



At the photolysis fluences employed ( $\sigma I = 0.02 - 0.03$ ), Process (6) is expected to make a lesser contribution to the observed decay than Process (5). In addition,  $\text{NF}(X^3\Sigma)$  is itself removed by

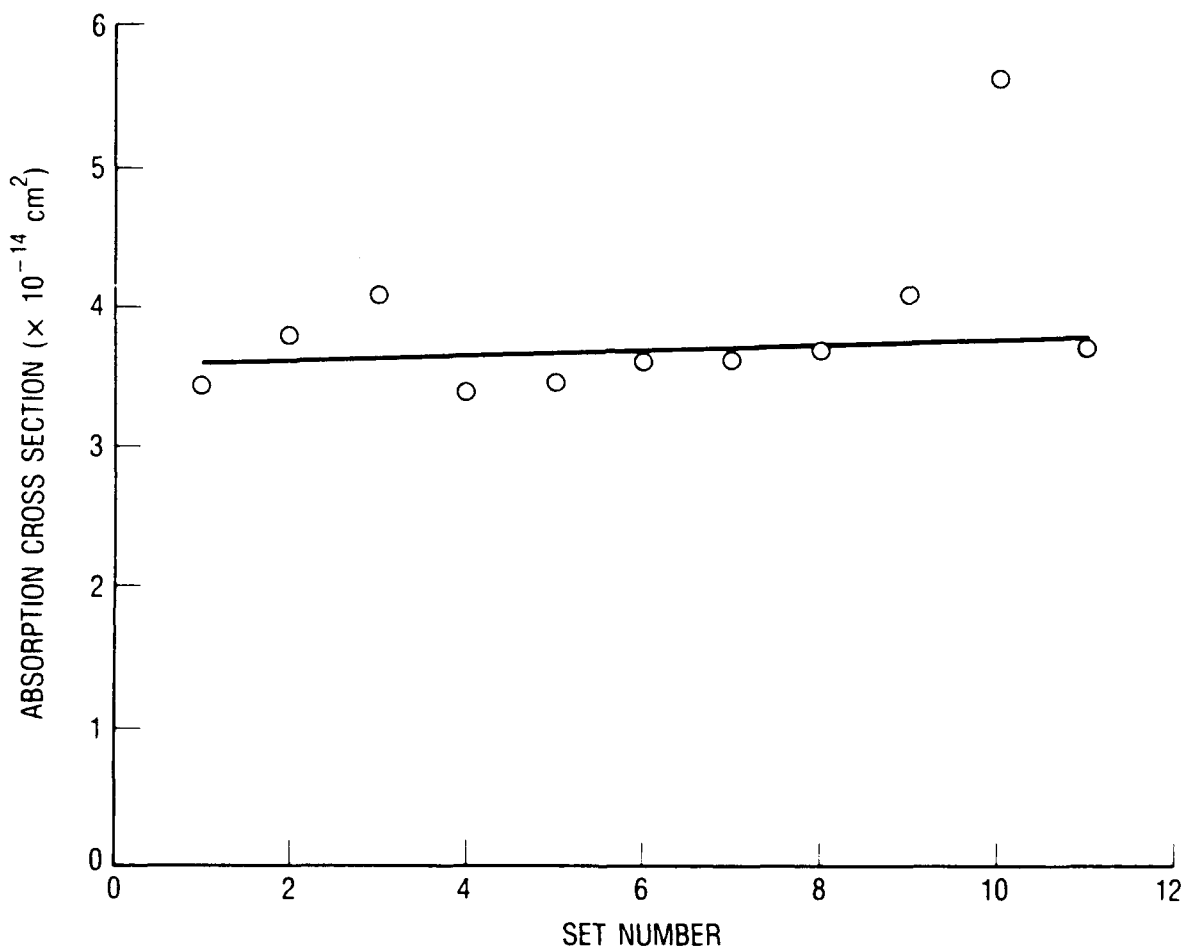


Fig. 6. Experimental Determinations of the Absorption Cross Section  $\sigma$  for the  $7s \ ^4P_{3/2} \leftarrow 6p^3 \ ^2D_{3/2}$  Bi Atom Transition at 298.99 nm. A value of  $\sigma = 3.7 \pm 1.4 \times 10^{-14} \text{ cm}^2$  was obtained. This is to be compared to a theoretical value of  $5 \times 10^{-12} \text{ cm}^2$  based on the oscillator strength of the transition.

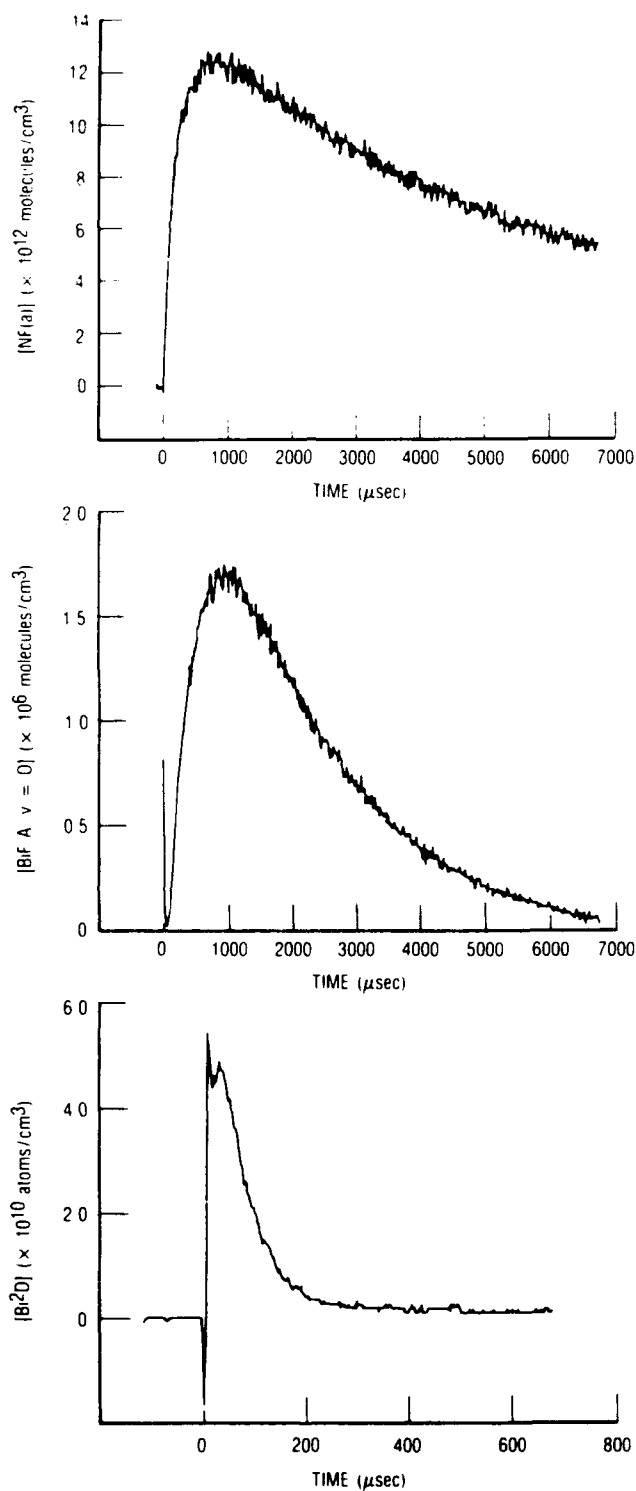


Fig. 7. Experimental  $\text{NF}(a^1\Delta)$ ,  $\text{BiF}(A0^+)$ , and  $\text{Bi}(^2D_{3/2})$  Time Profiles. Species densities were  $[\text{NF}_2] = 1.5 \times 10^{15}$ ,  $[\text{Bi}(\text{CH}_3)_3] = 2.0 \times 10^{13}$ ,  $[\text{H}_2] = 4.3 \times 10^{14}$ ,  $[\text{CO}_2] = 7.1 \times 10^{16}$ , and  $[\text{Ar}] = 1.1 \times 10^{17}$ . The cell temperature was  $166^\circ\text{C}$ . The KrF photolysis laser was operated at 2 Hz and delivered a flux of about  $30 \text{ mJ/cm}^2$ . The traces are the average 25 laser shots. The  $\text{Bi}(^2D_{3/2})$  trace was obtained from time-resolved LIF data. Note shorter time scale for the  $\text{Bi}(^2D_{3/2})$  data.

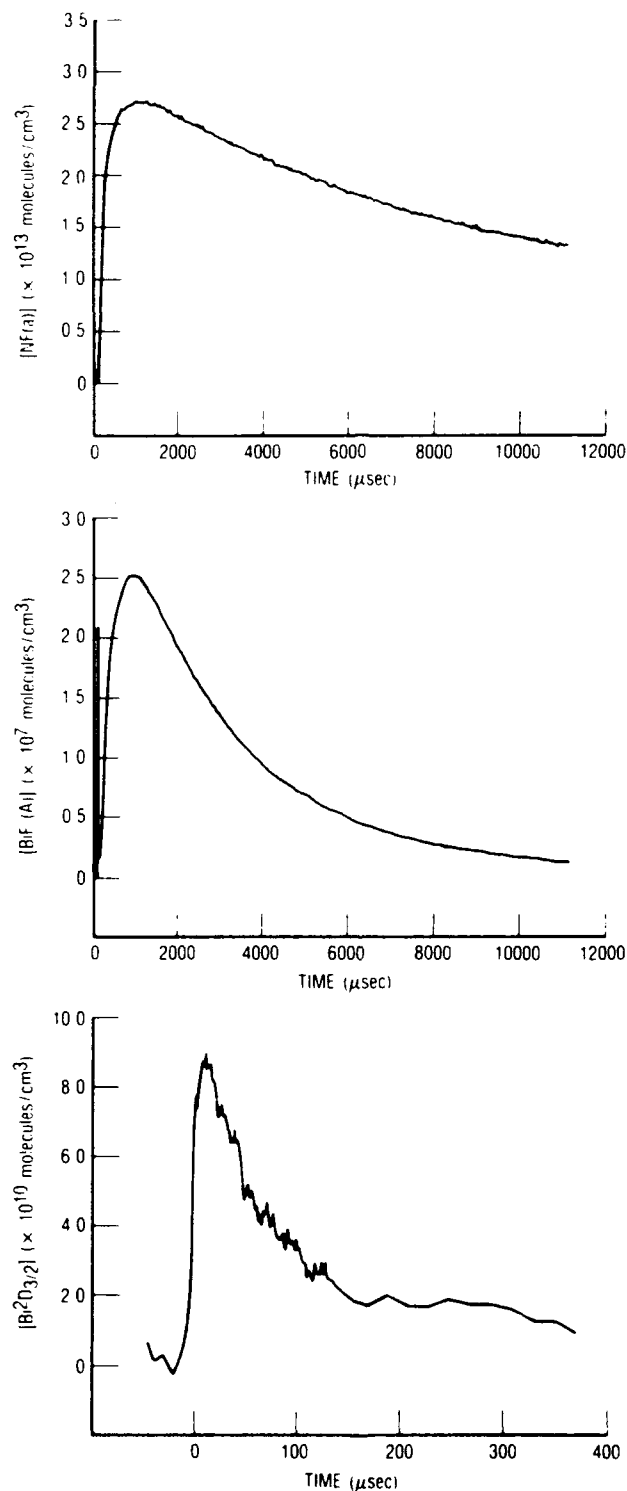


Fig. 8. Excited State Time Histories of  $\text{NF}(a^1\Delta)$ ,  $\text{BiF}(A0^+)$ , and  $\text{Bi}(^2D_{3/2})$ . The  $\text{Bi}(^2D_{3/2})$  trace was obtained from time-resolved absorption data. Reagent concentrations were  $[\text{NF}_2] = 1.5 \times 10^{15}$ ,  $[\text{Bi}(\text{CH}_3)_3] = 2.2 \times 10^{13}$ ,  $[\text{H}_2] = 1.1 \times 10^{15}$ , and  $[\text{CO}_2] = 5.0 \times 10^{17}$ . The cell was held at a total pressure of 8.25 torr with Ar and a temperature of 174°C. The KrF photolysis laser was operated at 2 Hz and delivered a flux of about 38 mJ/cm<sup>2</sup>. The traces are the average 100 laser shots. Note the shorter time scale for the  $\text{Bi}(^2D_{3/2})$  data.



on a relatively rapid ( $\sim 350 \mu\text{sec}$ ) timescale (Ref. 18). Recent measurements in this laboratory have determined that  $k_5 \leq 1.2 \times 10^{-11} \text{ cm}^3/\text{molecule}\cdot\text{sec}$ . If we take  $k_6 = 1.7 \times 10^{-10}$  (determined according to detailed balance from  $k_1 = 1.8 \times 10^{-10}$ ),  $k_7 = 2.0 \times 10^{-12}$ ,  $[\text{NF}(X^3\Sigma)]_0 = 3.2 \times 10^{13}$ , and  $[\text{NF}_2] = 1.4 \times 10^{15}$ , then the  $\text{Bi}(^2\text{D}_{3/2})$  decay rates are reasonably well modeled by consideration of Processes (5), (6), and (7) alone.

Under our conditions, the predominant manner of removal of  $\text{BiF}(\text{A}0^+)$  is spontaneous emission,



Proceeding on the assumption that Mechanism 2 is dominant and conditions are in steady state, on the basis of Processes (3), (4), and (8) one can conclude that

$$k_4 = A_{\text{BiF}}[\text{BiF}(\text{A}0^+)]/[\text{Bi}(^2\text{D}_{3/2})][\text{NF}(a^1\Delta)] \quad (\text{II})$$

where  $k_4$  is the rate constant for Process (4) and  $A_{\text{BiF}}$  is the  $\text{BiF}(\text{A} \rightarrow \text{X})$  Einstein A coefficient. Steady state conditions are attained when the rate of change of  $[\text{NF}(a^1\Delta)]$  and  $[\text{Bi}(^2\text{D}_{3/2})]$  is small compared to the radiative loss  $\text{BiF}(\text{A}0^+)$ . For these experiments, this condition was met in all cases. Thus, if  $\text{BiF}(\text{A}0^+)$  is formed primarily by Mechanism 2, one would expect plots constructed from  $\text{BiF}(\text{A}0^+)$ ,  $\text{Bi}(^2\text{D}_{3/2})$ , and  $\text{NF}(a^1\Delta)$  experimental time profiles using Eq. (II) to have a constant magnitude equal to  $k_4$ . Figure 9 presents a plot of Eq. (II) for the data in Fig. 8 at early times. This plot does not reach a constant value, but rather continues to increase with time. Clearly this result is in conflict with Eq. II. Either the assumption of a steady-state condition is not justified, or else Mechanism 2 as written is not the principal method of  $\text{BiF}(\text{A}0^+)$  production under our conditions.

A kinetic model developed by Herbelin<sup>†</sup> was used to calculate  $\text{Bi}(^2\text{D}_{3/2})$ ,  $\text{NF}(a^1\Delta)$ , and  $\text{BiF}(\text{A}0^+)$  time profiles using the isothermal NIST ACUCHEM numerical modeling code (Ref. 19). The initial conditions employed were identical to the experimental conditions in Fig. 8. The sole  $\text{BiF}(\text{A}0^+)$  production step in this model is the  $\text{Bi}(^2\text{D}_{3/2}) + \text{NF}(a^1\Delta)$  reaction, and the predominant  $\text{BiF}(\text{A}0^+)$  removal is radiative. The reactions and rate coefficients used in this model are presented in the appendix. Figure 10 shows a steady-state plot suggested by Eq. (II) calculated with this model for the same time frame as portrayed in Fig. 9. This plot rapidly reaches a constant value which is in good agreement with the value of  $k_4$  ( $7.8 \times 10^{-11} \text{ molecule}/\text{cm}^3\cdot\text{sec}$ ) input into the calculations. Thus, a steady-state assumption is valid, even when applied to a more detailed kinetic analysis of this system.

It is therefore necessary to question the validity of the mechanism. The  $\text{BiF}(\text{A}0^+)$  time behavior portrayed in Figs. 7 and 8 is not consistent with Mechanism 2. According to Reactions (3)

<sup>†</sup> J. M. Herbelin, private communication, The Aerospace Corporation, El Segundo, CA.

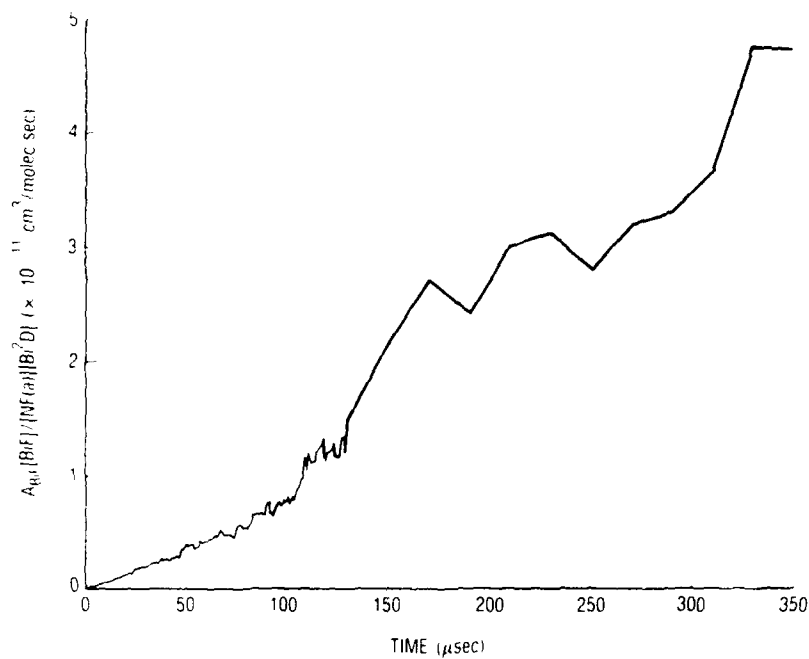


Fig. 9. Plot of Eq. (II) Constructed from the Absolute Data Presented in Fig. 8. The data from  $\text{BiF}(\text{AO}^+)$  used in this plot have had the scattered-light spike subtracted; an extrapolation from the remaining data was used for  $t < 30 \mu\text{sec}$ .

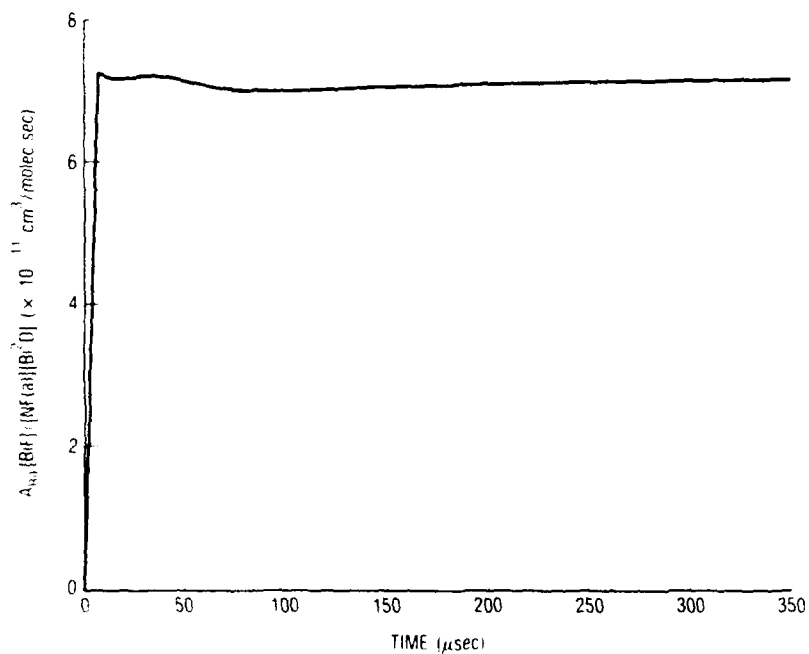


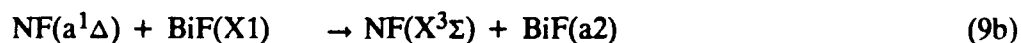
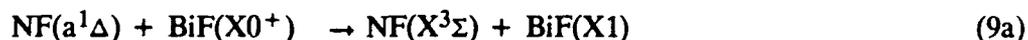
Fig. 10. Steady-State Plot Suggested by Eq. (II) Calculated Using the Kinetic Model Presented in the Appendix. The initial conditions are the same as for Fig. 8.

and (4), and Process (8), the peak concentration of  $\text{BiF}(\text{A}0^+)$  should occur when the  $\text{Bi}(^2\text{D}_{3/2})$  and  $\text{NF}(\text{a}^1\Delta)$  densities cross. Further, the  $\text{BiF}(\text{A}0^+)$  density should fall off rapidly as  $\text{Bi}(^2\text{D}_{3/2})$  decreases.  $\text{Bi}(^2\text{D}_{3/2})$  does appear to reach a steady-state concentration at long times ( $> 200 \mu\text{sec}$ ) but at a level that is at the lower limit of our dynamic range for these measurements. The significance of this long time behavior is uncertain. It may well represent establishment of an equilibrium with  $\text{NF}(\text{a}^1\Delta)$ . Whether it is also in equilibrium with  $\text{BiF}(\text{A}0^+)$  by Reaction (4a) or suppressed by means of Processes such as (4b) and (5) is impossible to determine within the context of these experiments. The following conclusions may be drawn, however:

- At the densities employed here,  $\text{Bi}(^2\text{D}_{3/2})$  is formed directly during the photolysis pulse and by cascading from higher lying states;
- $\text{Bi}(^2\text{D}_{3/2})$  is efficiently removed, probably by reactive collisions with  $\text{NF}_2$ ;
- $\text{Bi}(^2\text{D}_{3/2})$  does appear to reach a steady-state density in equilibrium with  $\text{NF}(\text{a}^1\Delta)$  at relatively long times, but at a level far below that which modeling predicts;
- $\text{Bi}(^2\text{D}_{3/2})$  does not display a temporal behavior that is compatible with the production of  $\text{BiF}(\text{A}0^+)$  by Process (4a).

Hence, we conclude that  $\text{BiF}(\text{A}0^+)$  formation under these conditions cannot be accounted for solely by Mechanism 2.

Balasubramanian has published a theoretical study of the low-lying electronic states of  $\text{BiF}$  (Ref. 20). More recently, Vervloet et al.\* have analyzed experimental FTIR spectra of  $\text{BiF}$  which fixed  $T_e$  for the X1 state at a significantly higher value than we had estimated earlier (Ref. 4). This assignment appears to substantiate the general features calculated by Balasubramanian. In particular, three of the four lowest lying states arising from the  $\sigma^2 \pi^4 \pi^{*2}$  configuration appear to be determined. These assignments are presented in a revised potential energy diagram in Fig. 11. Since all of Balasubramanian's calculated term values appear to be high by 2000 to 3000  $\text{cm}^{-1}$ , it is not unreasonable to assume that the a2 state is located in the region of 11500 to 12500  $\text{cm}^{-1}$ . If this is the case, an argument can be made that the  $\text{BiF}^*$  state of Mechanism 1 is actually the a2 state. The substantially higher electronic term value of the a2 state (in comparison to that of the  $\text{b}0^+$  state suggested by Ref. 2) removes the constraint of invoking a vibrationally excited intermediate. This in turn leaves our previous conclusions (Ref. 4) open for reassessment. Our current results lead us to believe that some variation of Mechanism 1 must be the operative pathway to  $\text{BiF}(\text{A}0^+)$  production. Certainly Process (2) must be the final step; however, there is no evidence to preclude the possibility of such processes as



contributing to the overall production of the intermediate a2 state.

---

\*M. Vervloet, Herzberg Institute of Astrophysics, National Research Council of Canada, Ottawa, Canada, private communication.

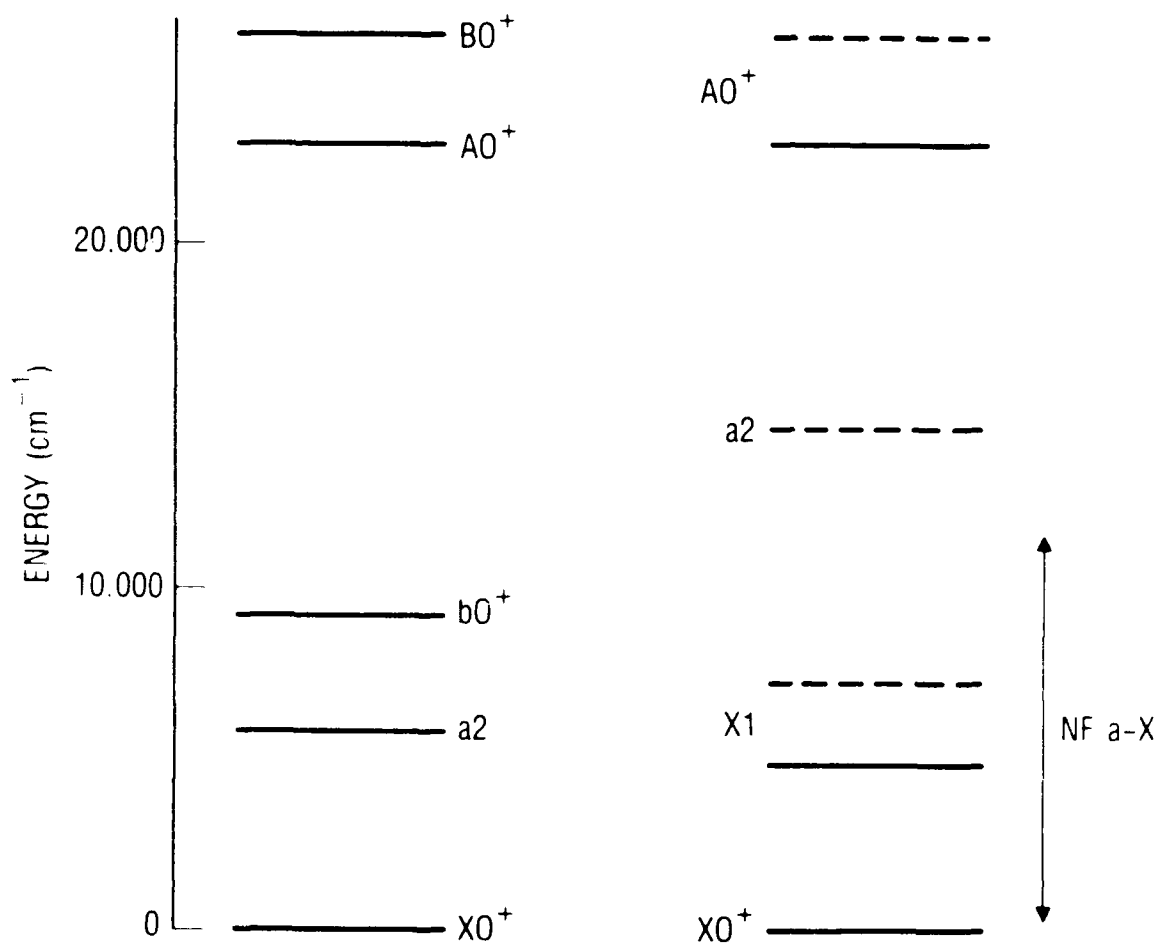
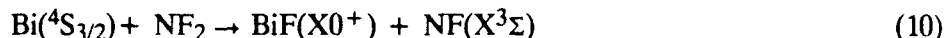


Fig. 11. Zero-Point Energies of the Lowest Lying States of BiF According to Ref. 2 (on the left) and the More Recent Assignment of Ref. 20 (on the right). The energy of NF(a-X) is also indicated. The diagram on the right uses dashed lines to indicate theoretical assignments and solid lines for states that have been experimentally observed.

We have not yet specified the origin of  $\text{BiF}(\text{X}0^+)$  in Mechanism 1. Under the conditions of our experiments, the  $\text{NF}_2$  density is in substantial excess. The  $\text{NF-F}$  and  $\text{Bi-F}$  bond energies were thought to be comparable; however, analysis of recent spectroscopic evidence (Ref. 21) suggests a  $\text{BiF}(\text{X})$  bond energy of 100 kcal/mol. Thus, the most plausible source of ground state  $\text{BiF}$  is



In addition, processes such as Reactions (4b) and (5b) may also contribute  $\text{BiF}(\text{A}0^+)$  formation in the system by channeling excited state intermediates into the production cycle. The short radiative lifetime of the  $\text{A}0^+$  state quickly leads to an equilibrium concentration of ground state  $\text{BiF}$ . We discount Reaction (5a) as being a major source of  $\text{BiF}(\text{X}0^+)$  on the basis of experimental data (Ref. 4) which show time histories of  $\text{BiF}(\text{X}0^+)$  that rise with time constants on the order of 100 to 150  $\mu\text{sec}$ . At the concentrations of  $\text{NF}_2$  employed in those experiments ( $10^{16}$  molecules/ $\text{cm}^3$ ), our rate for  $k_5$  would dictate rise times on the order of 5 to 10  $\mu\text{sec}$ . These observations are confirmed qualitatively by modeling calculation with the ACUCHEM and NEST codes.

It is of interest to consider the total number of  $\text{BiF A-X}$  photons emitted as a function of initial conditions. When examined with respect to the  $\text{NF}(a^1\Delta)$  density, such a quantity leads to a better understanding of the global efficiency of this system since it is directly related to how the chemical energy stored in  $\text{NF}(a^1\Delta)$  is converted into  $\text{BiF A-X}$  photons. Energy considerations dictate that at least two  $\text{NF}(a^1\Delta)$  molecules are required for the production of a single  $\text{BiF A-X}$  photon. However, processes such as electronic quenching of  $\text{NF}(a^1\Delta)$  or  $\text{BiF}(\text{A}0^+)$  and  $\text{NF}(a^1\Delta)$  reactions with  $\text{Bi}(\text{CH}_3)_3$  will serve to limit the efficiency. The extent to which  $\text{Bi}$  atoms are recycled through the reaction system can be estimated from the initial  $\text{Bi}$  atom density resulting from the multiphoton  $\text{Bi}(\text{CH}_3)_3$  photolysis.

The absolute number of  $\text{NF}(a^1\Delta)$  molecules is constrained by the initial  $\text{H}_2$  density under conditions where  $[\text{NF}_2]_0 \gg [\text{H}_2]_0$ . If  $[\text{F}]_0 > [\text{H}_2]_0$ , one will see  $[\text{NF}(a^1\Delta)]_{\text{max}} \leq 0.9 [\text{H}_2]_0$ . If  $[\text{F}]_0 < [\text{H}_2]_0$ , the  $\text{NF}_2/\text{H}_2$  chain will run and  $[\text{NF}(a^1\Delta)]_{\text{max}} = C([\text{F}]_0 + [\text{NF}(\text{X}^3\Sigma^-)])$ , as discussed in Ref. 11. In this latter case, it is a bit more difficult to quantify the total  $\text{NF}(a^1\Delta)$  produced. The total number of  $\text{BiF A-X}$  photons is relatively easy to measure.

To minimize the effect of  $\text{NF}(a^1\Delta)$  reactions with  $\text{Bi}(\text{CH}_3)_3$ , a series of experiments were performed with  $\text{NF}(a^1\Delta)$  densities an order of magnitude larger than  $[\text{Bi}(\text{CH}_3)_3]$ . The total  $\text{BiF A-X}$  photon emission is calculated using our  $\text{BiF A-X}$  ( $v' = 0, v'' = 2$ ) emission data and the  $\text{A-X}(0,2)$  Franck-Condon factor (Ref. 2). The  $\text{BiF}(\text{A})$  state was assumed to be in vibrational equilibrium at our operating temperature of 440 K. The photodissociation dynamics of  $\text{Bi}(\text{CH}_3)_3$  are unknown. However, bond strength considerations (Ref. 22) show that a  $\text{KrF}$  photon has sufficient energy to break all the  $\text{Bi-CH}_3$  bonds and produce a  $\text{Bi}$  atom in its ground state. Production of excited  $\text{Bi}$  requires at least two  $\text{KrF}$  photons. Hence, an upper limit of the initial  $\text{Bi}$  atomic densities can be obtained from the  $\text{Bi}(\text{CH}_3)_3$  absorption cross section at 249 nm (Ref. 16) and the  $\text{KrF}$  flux. The results are presented in Table 1. The maximum  $\text{BiF A-X}$  photon production efficiency is on the order of 4%, where 100% efficiency would result in the production of one  $\text{BiF A-X}$  photon for every two  $\text{NF}(a^1\Delta)$  molecules in the system. It may also be noted that about two  $\text{BiF A-X}$  photons result for each  $[\text{Bi}]_0$ . Thus we observe evidence of repetitive pumping of  $\text{Bi}$  (either as  $\text{BiF}$  or in the atomic form). Our earlier data (Ref. 4) demonstrated a finite appearance time for ground

state Bi <sup>4</sup>S atoms upon KrF photolysis of Bi(CH<sub>3</sub>)<sub>3</sub>. This suggests that the photolysis results in mostly excited Bi and therefore requires at least two photons. If this is the case, our estimate of [Bi]<sub>0</sub> will be low, and both conversion efficiency and the extent of recycling will be underestimated. On the other hand, multiple reactions with Bi(CH<sub>3</sub>)<sub>3</sub> may introduce additional Bi/BiF into the system at times that are long with respect to the initial photolysis pulse. Note that these observations are general in nature. They do not depend on a knowledge of the production mechanism of BiF(A0<sup>+</sup>).

Accurate knowledge of the BiF(A0<sup>+</sup>) formation mechanism is necessary in order to effectively evaluate the efficiency of the system. There are certain loss processes, however, that would be common to either route. The most significant among these are



It is clear, from the data taken on all approaches to BiF(A0<sup>+</sup>) scaling, that the energy extraction efficiency improves as precursor species such as NF<sub>2</sub> or Bi(CH<sub>3</sub>)<sub>3</sub> (at constant [Bi]) are reduced with respect to NF(a<sup>1</sup>Δ).<sup>7</sup> This is to be expected for either mechanism. The other processes that lead to a lower efficiency will be those that remove the BiF(A0<sup>+</sup>) precursor [i.e., Bi(<sup>2</sup>D<sub>3/2</sub>) or BiF(a2)] or those that represent poor branching ratios (e.g., k<sub>4a</sub> << k<sub>4b</sub> for Mechanism 2).

Table 1. Total Integrated BiF(A) Photon Emission

Run No.	[NF(a)] <sub>0</sub> <sup>a</sup>	[Bi] <sup>b</sup>	Total BiF A-X Photons <sup>c</sup>
1	1.9 × 10 <sup>14</sup>	≤ 1.4 × 10 <sup>12</sup>	2.2 × 10 <sup>12</sup>
2	2.5 × 10 <sup>14</sup>	≤ 1.5 × 10 <sup>12</sup>	3.6 × 10 <sup>12</sup>
3	1.5 × 10 <sup>14</sup>	≤ 1.5 × 10 <sup>12</sup>	1.5 × 10 <sup>12</sup>
4	2.3 × 10 <sup>14</sup>	≤ 6.8 × 10 <sup>11</sup>	1.7 × 10 <sup>12</sup>
5	1.7 × 10 <sup>14</sup>	≤ 2.8 × 10 <sup>12</sup>	3.5 × 10 <sup>12</sup>

<sup>a</sup>Units of molecules/cm<sup>3</sup>.

<sup>b</sup>Units of atoms/cm<sup>3</sup>. Upper limits using Bi(CH<sub>3</sub>)<sub>3</sub> absorption cross section (see text).

<sup>c</sup>Units of photons/cm<sup>3</sup>.

## V. CONCLUSIONS

Time profiles of  $\text{BiF}(A0^+)$ ,  $\text{Bi}(^2D_{3/2})$ , and  $\text{NF}(a^1\Delta)$  were monitored following KrF laser initiation of  $\text{NF}_2/\text{H}_2/\text{Bi}(\text{CH}_3)_3/\text{Ar}/\text{CO}_2$  mixtures. Detection of all three species was calibrated absolutely to allow quantitative measurements of transient number densities to be made. For all conditions employed, the observed  $\text{BiF}(A0^+)$  and  $\text{Bi}(^2D_{3/2})$  time behavior was not consistent with the currently accepted mechanism for the production of  $\text{BiF}(A0^+)$ . While much work has already been done, more work on this system is needed in order to provide a more complete understanding of reactions leading to  $\text{BiF}(A0^+)$ . In particular, spectroscopic characterization of the low lying BiF electronic states is necessary so that their role in the kinetics of this system can be fully evaluated. The relaxation and removal processes involving the BiF ground state must be studied before the mass efficiency and operating characteristics of this potential laser can be effectively judged.

## REFERENCES

1. J. M. Herbelin and R. A. Klingberg, *Int. J. Chem. Kinetics* **16**, 849 (1984)
2. W. E. Jones and T. D. McLean, *J. Mol. Spectrosc.* **90**, 481 (1981).
3. K. J. Chakoo and M. M. Patel, *Indian J. Pure Appl. Phys.* **17**, 189 (1979)
4. R. F. Heidner III and J. B. Koffend, *Time-Resolved Kinetics of the NF\*–BiF Candidate Chemical Laser System*, TOR-0086(6604)-1, The Aerospace Corporation, El Segundo, CA (1986)
5. G. A. Capelle, D. G. Sutton, and J. I. Steinfeld, *J. Chem. Phys.* **69**, 5140 (1978)
6. G. A. W. Rutgers and J. C. DeVos, *Physics XX*, 715 (1954).
7. J. F. Bott, C. E. Gardner, R. F. Heidner, J. M. Herbelin, R. Hofland, Jr., J. S. Holloway, J. B. Koffend, M. A. Kwok, R. H. Ueunten, S. T. Amimoto, and G. N. Harper, *Pulsed Photolytic Density Scaling Experiment for BiF*, TR-0088(3604)-2, The Aerospace Corporation, El Segundo, CA (1988).
8. J. Garstang, *J. Res. Natl. Bur. Stand.* **68A**, 61 (1964)
9. R. F. Heidner III, H. Helvajian, J. S. Holloway, and J. B. Koffend, *J. Chem. Phys.* **84**, 2137 (1986).
10. R. J. Malins and D. W. Setser, *J. Chem. Phys.* **85**, 1342 (1981).
11. J. B. Koffend, C. E. Gardner, and R. F. Heidner III, *J. Chem. Phys.* **83**, 2904 (1985).
12. R. F. Heidner III, H. Helvajian, and J. B. Koffend, *J. Chem. Phys.* **87**, 1520 (1987).
13. F. Magnotta, D. J. Nesbitt, and S. R. Leone, *Chem. Phys. Lett.* **83**, 21 (1981)
14. R. F. Heidner III, H. Helvajian, J. S. Holloway, and J. B. Koffend, *J. Chem. Phys.* **93**, 7818 (1989).
15. C. H. Corliss and W. R. Bozman, *Experimental Transition Probabilities for Spectral Lines of Seventy Elements*, NBS Monograph 53, 14 (1962).
16. J. S. Holloway, J. B. Koffend, and R. F. Heidner, *J. Chem. Phys.* **93**, 7665 (1989).
17. B. A. Palmer, R. A. Keller, and R. Engleman, Jr., *An Atlas of Uranium Emission Intensities in a Hollow Cathode Discharge*, LA-8251-MS Informal Report, UC-34a, UC-LASL (July 1980).
18. R. F. Heidner III, H. Helvajian, J. S. Holloway, and J. B. Koffend, *J. Chem. Phys.* **93**, 7813 (1989).
19. W. Braun and J. T. Herron, "ACUCHEM", a Computer Program for Modeling Complex Reaction Systems, NIST, Gaithersburg, MD (1986).
20. K. Balasubramanian, *Chem. Phys. Lett.* **127**, 324 (1986).

## REFERENCES (Continued)

21. A. J. Ross, R. Bacis, J. d'Incan, C. Effantin, J. B. Koffend, A. Toupouzkhania, and J. Verges, *Chem. Phys. Lett.*, to be published.
22. S. J. W. Price and A. F. Trotman-Dickenson, *Trans. Farad. Soc.*, 1630 (1958).

APPENDIX: KINETIC MODEL<sup>a</sup>NF<sub>2</sub> REACTIONS

Reaction			Rate Constant <sup>b</sup>
F + H <sub>2</sub>	→	HF + H	3.7 × 10 <sup>-11</sup>
H + NF <sub>2</sub>	→	HF + NF(a)	1.3 × 10 <sup>-11</sup>
H + NF <sub>2</sub>	→	HF + NF(b)	2.8 × 10 <sup>-13</sup>
H + NF <sub>2</sub>	→	HF + NF(X)	1.0 × 10 <sup>-12</sup>
H + NF(a)	→	HF + N	1.26 × 10 <sup>-11</sup>

## NF REACTIONS

Reaction			Rate Constant <sup>b</sup>
N + NF(a)	→	N <sub>2</sub> + F	3.0 × 10 <sup>-11</sup>
NF(X) + NF(X)	→	N <sub>2</sub> + F + F	2.0 × 10 <sup>-12</sup>
NF(a) + NF(a)	→	N <sub>2</sub> + F + F	2.0 × 10 <sup>-12</sup>
NF(X) + NF(a)	→	N <sub>2</sub> + F + F	2.0 × 10 <sup>-12</sup>
NF(a) + Ar	→	NF(X) + Ar	2.7 × 10 <sup>-16</sup>
N + NF <sub>2</sub>	→	NF(X) + NF(X)	4.6 × 10 <sup>-12</sup>
NF(X) + NF <sub>2</sub>	→	F + N <sub>2</sub> F <sub>2</sub>	2.4 × 10 <sup>-12</sup>
NF(a) + NF <sub>2</sub>	→	F + N <sub>2</sub> F <sub>2</sub>	2.7 × 10 <sup>-16</sup>

<sup>a</sup>This kinetic rate package is a working version of an ongoing effort to accurately model the chemistry of the NF/BiF system. It is presented to demonstrate the applicability of the steady-state assumption under the premise that Mechanism 2 is operative. It does not represent the most current version that the model has assumed. The authors are indebted to J. M. Herbelin for his permission to include it here.

<sup>b</sup>cm<sup>3</sup>/molecule-sec

NF(a)/Bi<sup>4</sup>S)/BiF REACTIONS

Reaction			Rate Constant <sup>a</sup>
NF(a) + Bi( <sup>4</sup> S)	→	NF(X) + Bi( <sup>2</sup> D)	$1.9 \times 10^{-10}$
NF(X) + Bi( <sup>2</sup> D)	→	NF(a) + Bi( <sup>4</sup> S)	$1.9 \times 10^{-10}$
NF(a) + Bi( <sup>2</sup> D)	→	N + BiF(A)	$7.80 \times 10^{-11}$
NF(a) + BiF(A)	→	N + BiF <sub>2</sub>	$5 \times 10^{-10}$
BiF(A)	→	BiF(X) + hν	<sup>b</sup> $7 \times 10^5$
BiF(A) + Ar	→	BiF(X) + Ar	$4.5 \times 10^{-13}$
BiF(X) + H	→	Bi( <sup>4</sup> S) + HF	$4.0 \times 10^{-11}$
BiF(X) + NF(a)	→	Bi( <sup>4</sup> S) + NF <sub>2</sub>	$1.2 \times 10^{-10}$
BiF(X) + NF(X)	→	Bi( <sup>4</sup> S) + NF <sub>2</sub>	$1.2 \times 10^{-10}$

Bi/NF<sub>2</sub> REACTIONS

Reaction			Rate Constant <sup>a</sup>
Bi( <sup>4</sup> S) + NF <sub>2</sub>	→	BiF(X) + NF(X)	$5.0 \times 10^{-12}$
Bi( <sup>2</sup> D) + NF <sub>2</sub>	→	BiF(a) + NF(X)	$\leq 1.2 \times 10^{-11}$
BiF(X) + NF <sub>2</sub>	→	BiF <sub>2</sub> + NF(X)	$5.0 \times 10^{-14}$
BiF <sub>2</sub> + Bi	→	BiF(X) + BiF(X)	$5 \times 10^{-12}$

<sup>a</sup>cm<sup>3</sup>/molecule-sec

<sup>b</sup>sec<sup>-1</sup>

Bi(CH<sub>3</sub>)<sub>3</sub> DISSOCIATION PROCESSES

Reaction	→	Rate Constant <sup>a</sup>
NF(a) + Bi(CH <sub>3</sub> ) <sub>3</sub>	→	NF(X) + Bi(CH <sub>3</sub> ) <sub>3</sub> <sup>*</sup> 2.7 × 10 <sup>-11</sup>
NF(a) + Bi(CH <sub>3</sub> ) <sub>2</sub>	→	NF(X) + Bi(CH <sub>3</sub> ) <sub>2</sub> <sup>*</sup> 2.7 × 10 <sup>-11</sup>
NF(a) + BiCH <sub>3</sub>	→	NF(X) + BiCH <sub>3</sub> <sup>*</sup> 2.7 × 10 <sup>-11</sup>
NF(a) + Bi(CH <sub>3</sub> ) <sub>3</sub> <sup>*</sup>	→	Bi(CH <sub>3</sub> ) <sub>3</sub> <sup>**</sup> + NF(X)      2.7 × 10 <sup>-11</sup>
NF(a) + Bi(CH <sub>3</sub> ) <sub>2</sub> <sup>*</sup>	→	NF(X) + Bi(CH <sub>3</sub> ) <sub>2</sub> <sup>**</sup> 2.7 × 10 <sup>-11</sup>
Bi(CH <sub>3</sub> ) <sub>3</sub> <sup>*</sup>	→	Bi(CH <sub>3</sub> ) <sub>2</sub> + CH <sub>3</sub> <sup>b</sup> 2.7 × 10 <sup>4</sup>
Bi(CH <sub>3</sub> ) <sub>2</sub> <sup>*</sup>	→	BiCH <sub>3</sub> + CH <sub>3</sub> <sup>b</sup> 1.9 × 10 <sup>7</sup>
Bi(CH <sub>3</sub> ) <sup>*</sup>	→	Bi( <sup>4</sup> S) + CH <sub>3</sub> <sup>b</sup> 2.8 × 10 <sup>12</sup>
Bi(CH <sub>3</sub> ) <sub>3</sub> <sup>*</sup>	→	Bi(CH <sub>3</sub> ) <sub>2</sub> <sup>*</sup> + CH <sub>3</sub> <sup>b</sup> 4.7 × 10 <sup>7</sup>
Bi(CH <sub>3</sub> ) <sub>2</sub> <sup>**</sup>	→	BiCH <sub>3</sub> <sup>*</sup> + CH <sub>3</sub> <sup>b</sup> 2.26 × 10 <sup>10</sup>
Bi(CH <sub>3</sub> )	→	Bi( <sup>4</sup> S) + CH <sub>3</sub> <sup>b</sup> 5 × 10 <sup>5</sup>
Bi(CH <sub>3</sub> ) <sub>3</sub> <sup>**</sup> + Ar	→	Bi(CH <sub>3</sub> ) <sub>3</sub> <sup>*</sup> + Ar      4.0 × 10 <sup>-14</sup>
BiCH <sub>3</sub> ) <sub>3</sub> <sup>*</sup> + Ar	→	Bi(CH <sub>3</sub> ) <sub>3</sub> + Ar      4.0 × 10 <sup>-14</sup>
Bi(CH <sub>3</sub> ) <sub>2</sub> <sup>**</sup> + Ar	→	Bi(CH <sub>3</sub> ) <sub>2</sub> <sup>*</sup> + Ar      4.0 × 10 <sup>-14</sup>
Bi(CH <sub>3</sub> ) <sub>2</sub> <sup>*</sup> + Ar	→	Bi(CH <sub>3</sub> ) <sub>2</sub> + Ar      4.0 × 10 <sup>-14</sup>

<sup>a</sup>cm<sup>3</sup>/molecule-sec

<sup>b</sup>sec<sup>-1</sup>

### Bi(<sup>2</sup>D) QUENCHING REACTIONS

Reaction	Rate Constant <sup>a</sup>
Bi( <sup>2</sup> D) + H <sub>2</sub> → Bi( <sup>4</sup> S) + H <sub>2</sub>	2.0 × 10 <sup>-14</sup>
Bi( <sup>2</sup> D) + CH <sub>3</sub> → Bi( <sup>4</sup> S) + CH <sub>3</sub>	2.6 × 10 <sup>-10</sup>
Bi( <sup>2</sup> D) + Bi(CH <sub>3</sub> ) <sub>3</sub> → Bi( <sup>4</sup> S) + Bi(CH <sub>3</sub> ) <sup>**</sup>	7.7 × 10 <sup>-11</sup>
Bi( <sup>2</sup> D) + Bi(CH <sub>3</sub> ) <sub>2</sub> → Bi( <sup>4</sup> S) + Bi(CH <sub>3</sub> ) <sub>2</sub> <sup>*</sup>	7.7 × 10 <sup>-11</sup>
Bi( <sup>2</sup> D) + BiCH <sub>3</sub> → Bi( <sup>4</sup> S) + BiCH <sub>3</sub> <sup>*</sup>	7.7 × 10 <sup>-11</sup>

### METHYL REACTIONS

Reaction	Rate Constant <sup>a</sup>
CH <sub>3</sub> + NF <sub>2</sub> → CH <sub>3</sub> NF <sub>2</sub>	2.0 × 10 <sup>-12</sup>
CH <sub>3</sub> + CH <sub>3</sub> → C <sub>2</sub> H <sub>6</sub>	4.0 × 10 <sup>-11</sup>
CH <sub>3</sub> + NF(a) → CN + HF	2.60 × 10 <sup>-10</sup>
CH <sub>3</sub> + NF(X) → CN + H <sub>2</sub>	2.6 × 10 <sup>-10</sup>
H + CH <sub>3</sub> → CH <sub>4</sub>	6.0 × 10 <sup>-11</sup>

<sup>a</sup>cm<sup>3</sup>/molecule-sec

## FLUORINE ATOM SIDE REACTIONS

Reaction	→	Rate Constant <sup>a</sup>
F + CH <sub>4</sub>	→	HF + CH <sub>3</sub> 1.3 × 10 <sup>-10</sup>
F + Bi(CH <sub>3</sub> ) <sub>3</sub>	→	Bi(CH <sub>3</sub> ) <sub>2</sub> + products      1 × 10 <sup>-10</sup>
F + Bi(CH <sub>3</sub> ) <sub>3</sub> *	→	Bi(CH <sub>3</sub> ) <sub>2</sub> + products      1 × 10 <sup>-10</sup>
F + Bi(CH <sub>3</sub> ) <sub>3</sub> **	→	Bi(CH <sub>3</sub> ) <sub>2</sub> + products      1 × 10 <sup>-10</sup>
F + Bi(CH <sub>3</sub> ) <sub>2</sub>	→	BiCH <sub>3</sub> + products      1 × 10 <sup>-10</sup>
F + Bi(CH <sub>3</sub> ) <sub>2</sub> *	→	BiCH <sub>3</sub> + products      1 × 10 <sup>-10</sup>
F + Bi(CH <sub>3</sub> ) <sub>2</sub> **	→	BiCH <sub>3</sub> + products      1 × 10 <sup>-10</sup>
F + BiCH <sub>3</sub>	→	BiF(X) + products      1 × 10 <sup>-10</sup>

---

<sup>a</sup>cm<sup>3</sup>/molecule-sec

## LABORATORY OPERATIONS

The Aerospace Corporation functions as an "architect-engineer" for national security projects, specializing in advanced military space systems. Providing research support, the corporation's Laboratory Operations conducts experimental and theoretical investigations that focus on the application of scientific and technical advances to such systems. Vital to the success of these investigations is the technical staff's wide-ranging expertise and its ability to stay current with new developments. This expertise is enhanced by a research program aimed at dealing with the many problems associated with rapidly evolving space systems. Contributing their capabilities to the research effort are these individual laboratories:

**Aerophysics Laboratory:** Launch vehicle and reentry fluid mechanics, heat transfer and flight dynamics; chemical and electric propulsion, propellant chemistry, chemical dynamics, environmental chemistry, trace detection; spacecraft structural mechanics, contamination, thermal and structural control; high temperature thermomechanics, gas kinetics and radiation; cw and pulsed chemical and excimer laser development, including chemical kinetics, spectroscopy, optical resonators, beam control, atmospheric propagation, laser effects and countermeasures.

**Chemistry and Physics Laboratory:** Atmospheric chemical reactions, atmospheric optics, light scattering, state-specific chemical reactions and radiative signatures of missile plumes, sensor out-of-field-of-view rejection, applied laser spectroscopy, laser chemistry, laser optoelectronics, solar cell physics, battery electrochemistry, space vacuum and radiation effects on materials, lubrication and surface phenomena, thermionic emission, photosensitive materials and detectors, atomic frequency standards, and environmental chemistry.

**Electronics Research Laboratory:** Microelectronics, solid-state device physics, compound semiconductors, radiation hardening; electro-optics, quantum electronics, solid-state lasers, optical propagation and communications; microwave semiconductor devices, microwave/millimeter wave measurements, diagnostics and radiometry, microwave/millimeter wave thermionic devices; atomic time and frequency standards; antennas, rf systems, electromagnetic propagation phenomena, space communication systems.

**Materials Sciences Laboratory:** Development of new materials: metals, alloys, ceramics, polymers and their composites, and new forms of carbon; nondestructive evaluation, component failure analysis and reliability; fracture mechanics and stress corrosion; analysis and evaluation of materials at cryogenic and elevated temperatures as well as in space and enemy-induced environments.

**Space Sciences Laboratory:** Magnetospheric, auroral and cosmic ray physics, wave-particle interactions, magnetospheric plasma waves; atmospheric and ionospheric physics, density and composition of the upper atmosphere, remote sensing using atmospheric radiation; solar physics, infrared astronomy, infrared signature analysis; effects of solar activity, magnetic storms and nuclear explosions on the earth's atmosphere, ionosphere and magnetosphere; effects of electromagnetic and particulate radiations on space systems; space instrumentation.